ADVANCED MATERIALS
www.advmat.de

Photocatalytic Conversion of CO_2 into Renewable Hydrocarbon Fuels: State-of-the-Art Accomplishment, Challenges, and Prospects

Wenguang Tu, Yong Zhou, and Zhigang Zou**

Photocatalytic reduction of CO_2 into hydrocarbon fuels, an artificial photosynthesis, is based on the simulation of natural photosynthesis in green plants, whereby O_2 and carbohydrates are produced from H_2O and CO_2 using sunlight as an energy source. It couples the reductive half-reaction of CO_2 fixation with a matched oxidative half-reaction such as water oxidation, to achieve a carbon neutral cycle, which is like killing two birds with one stone in terms of saving the environment and supplying future energy. The present review provides an overview and highlights recent state-of-the-art accomplishments of overcoming the drawback of low photoconversion efficiency and selectivity through the design of highly active photocatalysts from the point of adsorption of reactants, charge separation and transport, light harvesting, and CO_2 activation. It specifically includes: i) band-structure engineering, ii) nanostructuralization, iii) surface oxygen vacancy engineering, iv) macro-/meso-/microporous structuralization, v) exposed facet engineering, vi) co-catalysts, vii) the development of a Z-scheme system. The challenges and prospects for future development of this field are also present.

1. Introduction

Photosynthesis uses solar light energy to couple the formation of O_2 and carbohydrates with the fixation of CO_2. This process produces a readily usable carbon source and an aerobic atmosphere to sustain almost all life on this planet. The center of this process is photosystem II (PSII), which photoinduces the water oxidation that provides a primary source of reducing equivalents (water-derived electrons and protons) to convert CO_2 into biomass, food, and fuel with an additional input of energy from photosystem I (PSI).[1] The idea of mimicking the overall natural photosynthetic cycle of chemical conversion of CO_2 into hydrocarbon fuels has been consistently drawing attention for more than 30 years, including biological conversion,[1] thermochemical conversion,[2] electrochemical conversion,[3] and photocatalytic reduction of CO_2.[4] During the conversion process, a high input of energy is needed for breaking the C=O bond due to the thermodynamic stability of CO_2. Compared with other methods, photocatalytic reduction of CO_2 into hydrocarbon fuels is a challenging, yet promising avenue for achieving a sustainable alternative to conventional fossil fuels with advantages as follows: i) it can be carried out in relatively mild conditions – room temperature and pressure; ii) this process uses a mass of abandoned CO_2 as the starting carbon source driven by inexhaustible and clean solar energy; iii) the photoreduction of CO_2 can directly generate short-chain hydrocarbon fuels such as CH_4, CH_3OH, C_2H_6 and so on, which can alleviate increasingly tense energy crisis; iv) the realization of this technology will make it possible to replace fossil fuels by CO_2 as C source in chemical industry. Therefore, photocatalytic reduction of CO_2 with H_2O into hydrocarbon fuels would be like killing two birds with one stone in terms of saving supplying energy and our environment.[5]

In spite of earlier reviews generally introducing the concept of artificial photosynthesis,[6–20] the present review beginning with a brief description of the basic principles of photocatalytic reduction of CO_2 provides an overview and highlights the state-of-the-art accomplishments of overcoming the drawback of low photoconversion efficiency and selectivity through the design of highly active photocatalysts from the point of view of adsorption of reactants, charge separation and transport, light harvesting, and CO_2 activation. It includes: i) band-stucture engineering, an effective approach to adjust bandgap and band position for utilizing solar energy effectively; ii) nanostructuralization, providing a direct pathway for electron transport, which is favorable for improving separation of photogenerated electron–hole pairs; ii) surface oxygen vacancy engineering, which is favorable for CO_2 adsorption and activation and changes the electronic and chemical properties of the semiconductor surfaces; iv) macro/meso/microporous structuralization, which results in readily access channel, and the large surface area that

Dr. W. Tu, Prof. Y. Zhou
Key Laboratory of Modern Acoustics
MOE, Institute of Acoustics
School of Physics
Nanjing University
22 Hankou Road, Nanjing, Jiangsu, 210093, P. R. China
E-mail: zhouyong1999@nju.edu.cn
Dr. W. Tu, Prof. Y. Zhou, Prof. Z. Zou
National Laboratory of Solid State Microstructures
School of Physics
Ecomaterials and Renewable Energy Research Center (ERERC)
Jiangsu Key Laboratory for Nano Technology
Nanjing University
22 Hankou Road, Nanjing, Jiangsu 210093, P. R. China
E-mail: zgzou@nju.edu.cn

DOI: 10.1002/adma.201400087

increases the adsorption of reactants and supplies more surface active sites; v) exposed facet engineering, which could adjust surface energy, surface active sites, and even electronic band structure; vi) co-catalysts, which can promote the separation and migration of photogenerated charge carriers, effectively lower the barrier for CO_2 activation, affect the selectivity of products, and inhibit the back-recombination reaction; vii) the development of a Z-scheme system that relies on both exploration of an efficient semiconductor photocatalyst and creation of active sites to promote surface chemical reactions in the presence of a redox mediator, and simultaneously suppress backward reactions involving redox mediator. The challenges and prospects for future development of this field are also present.

2. Basic Principles of Photocatalytic Reduction of CO_2

CO_2, a linear molecule, is one of most thermodynamically stable compounds of carbon. Photocatalytic reduction of CO_2 into hydrocarbon fuels demands input energy to break C=O bond and form C–H bond, involving the participation of multiple electrons and a corresponding number of protons.[21] Due to the highest chemical state (C^{4+}) of C atoms in CO_2, CO_2 can only be reduced with the support of reducing agents. H_2O is a preferred candidate of reducing agents compared with other ones such as H_2, S^{2-}, SO_3^{2-}, and amines, owing to its richness, non-toxicity, and effectiveness. Photocatalytic reduction of CO_2 with H_2O into hydrocarbon fuels such as CH_4 and CH_3OH is an uphill reaction with a highly positive change in Gibbs free energy: $CO_2 + 2H_2O \rightarrow CH_3OH + 3/2O_2$ ($\Delta G° = 702.2$ kJ mol^{-1}) and $CO_2 + 2H_2O \rightarrow CH_4 + 2O_2$ ($\Delta G° = 818.3$ kJ mol^{-1}). Thus, the input energy is used to overcome these reaction barriers, which is provided by incident light. The schematic illustration of basic mechanism of photocatalytic reduction of CO_2 is shown in **Figure 1**. In the photocatalytic processes, electrons are excited from the valence band (VB) to conduction band (CB) and an equal numbers of holes are generated in the CB simultaneously when semiconductor absorbs a flux of photons. The photogenerated electron–hole pairs separate from each other and vigorously move to catalytically active sites at semiconductor surface. At the surface of semiconductors, electrons

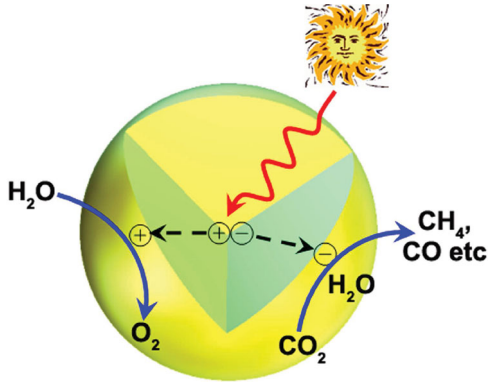

Figure 1. Schematic illustration of photoinduced generation of an electron–hole pair in semiconductor that transfers to the surface for CO_2 photoredox.

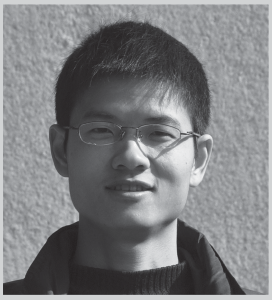

Wenguang Tu obtained his BS degree in 2010 from Southwest University, China. He is pursuing his Ph.D. degree under the guidance of Prof. Yong Zhou in ERERC, School of Physics, National Laboratory of Solid State Microstructures, Nanjing University, China. His current research involves the synthesis of graphene-based nanomaterials for photocatalysis application.

Yong Zhou studied chemistry and physics at the University of Science and Technology of China (USTC), and received his Ph.D. degree there in 2000. After working in Kyoto University in 2000–2001, the Max Planck Institute of Colloids and Interfaces in 2002–2003, the National Institute of Materials Science (NIMS) (Japan) in 2003–2004, the National Institute of Advanced Industrial Science and Technology (AIST) (Japan) in 2004–2008, and the National University of Singapore (NUS) in 2008–2009, he joined as a full professor in the Eco-materials and Renewable Energy Research Center (ERERC), School of Physics, National Laboratory of Solid State Microstructures, Nanjing University, China. His research now focuses on the design and fabrication of solar-light-driven clean energy materials for photocatalysis and flexible solar cells.

Zhigang Zou received his bachelors degree and masters degree from Tianjing University (China) in 1982 and 1986, respectively. He was a lecturer of Tianjing University from September 1986 to March 1991. Then, he moved to the Research Laboratory of Engineering Materials at the Tokyo Institute of Technology (Japan) as a visiting researcher. After he had received his Ph.D. degree from the University of Tokyo (Japan) in 1996, he was a researcher at the Photoreaction Control Research Center, National Institute of Advanced Industrial Science and Technology (AIST), Japan. He has been with the Department of Physics at Nanjing University (China) as a distinguished professor of the Chang Jiang Scholars Program since 2003. He is also a Director of the Ecomaterials and Renewable Energy Research Center, Nanjing University. His current research interests are photocatalysis, solar cells, and fuel cells.

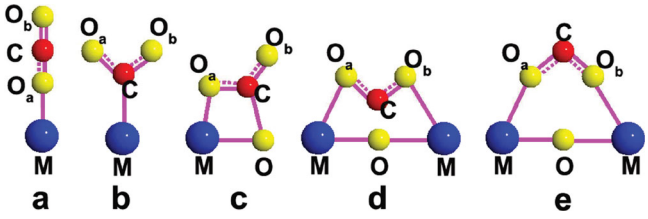

Figure 2. Possible configurations of adsorbed CO_2 on the photocatalyst surface.

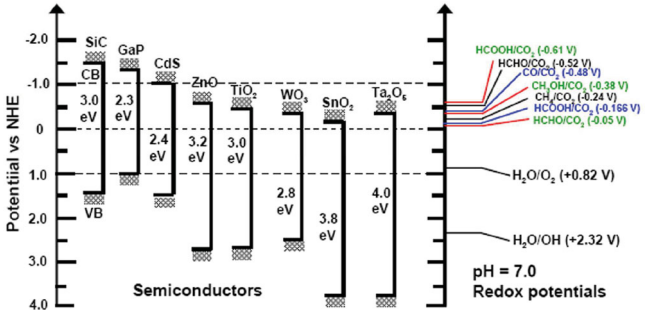

Figure 3. Conduction band, valence band potentials, and band gap energies of various semiconductor photocatalysts relative to the redox potentials at pH 7 of compounds involved in CO_2 reduction.

with reducing power reduce CO_2 into hydrocarbon fuels such as CO, CH_3OH, and CH_4 in the presence of H_2O, while the oxidation of H_2O occurs, owing to the oxidation ability of holes.[22] Through the chemical transformations, the abundant solar energy in the world can thus be effectively converted into chemical energy.

It was very essential to first understand the initial CO_2 absorption and activation mechanism so that effective photocatalysts could be devised to promote CO_2 reduction efficiency.[23,24] Five models are constructed for CO_2 absorption, and different absorption model determines the different adsorption energy of the system (**Figure 2**).[25] The first one is that the CO_2 molecule is linearly adsorbed on the surface via the O_a atom (Figure 2a). The second is that CO_2 molecule is absorbed via the C atom to generate a monodentate carbonate species (Figure 2b). In the third, a bidentate carbonate species is generated through interaction of a CO_2 molecule with the surface via both the O_a and C atom (Figure 2c). The fourth is the generation of a bridged carbonate geometry with the C atom of CO_2 pointing downward and two O atoms of CO_2 binding with two metal atoms to form a C···O bond with the O atom on the surface (Figure 2d). In the fifth, a bridging configuration with the C atom of CO_2 pointing upward and two O atoms of CO_2 binding with two metal atoms is formed (Figure 2e). The presence of an M–O–M bond on the surface is contributed to the formation of the fourth or the fifth model.

The activation of chemically stable CO_2 initiates multistep reactions for CO_2 reduction, which likely involves one electron transfer to CO_2 to generate $CO_2^{\bullet-}$ species by transferring an electron from excited photocatalysts to the lowest unoccupied molecular orbital (LUMO) of CO_2.[10,26–29] Accompanied with the acceptance of one electron, the transformation of CO_2 geometry from linear structure to a bent form also occurs significantly, owing to the repulsion among the two lone electron pairs on the oxygen atoms and the unpaired electron on the carbon atom.[30] The LUMO of CO_2 is lowered in energy upon decreasing the O-C-O bond angle from 180°.[10] The non-linear CO_2 molecule generated on the surface of solid bases is more destabilized than the linear CO_2 molecule, showing the high reactivity for CO_2 photoreduction.[31,32] Activated CO_2 is probably an important species in the photochemical reactions of CO_2. The transfer of one electron to free CO_2 is unfavorable thermodynamically, because the high LUMO level of CO_2 leads to a very negative redox potential for this process of $CO_2 + e^- \rightarrow CO_2^{\bullet-}$ (E^0_{redox} = –1.90 V, vs NHE), which has been proved by scanning tunneling microscopy experiments.[28,29] Thus, multiple electrons and a corresponding number of protons must involve the chemical reactions, reflecting the multicomponent steps observed in natural photosynthetic systems.[33] The formation of products can be different, decided by the number of electrons and protons taking part in the chemical reaction. CO is formed by reacting with two protons and two electrons, while CH_4 formation needs eight electrons and eight protons. The selectivity of products is one of considerable problems in the photocatalytic reduction of CO_2 process, which may be influenced by photocatalysts, reaction condition, and thermodynamic reduction potentials. **Figure 3** shows a schematic of different semiconductor photocatalysts relative to the redox potentials of different species. Two plausible pathways for CH_4 formation are proposed: i) $CO_2 \rightarrow HCOOH \rightarrow HCHO \rightarrow CH_3OH \rightarrow CH_4$; and ii) $CO_2 \rightarrow CO \rightarrow C^{\cdot} \rightarrow CH_2 \rightarrow CH_4$.[13,14] However, the understanding of photocatalytic mechanism and selectivity is still in infant due to complex multielectron-transfer process.[8,10,12]

3. State-of-the-Art Accomplishments of Design and Engineering of Highly Active Photocatalysts

Reducing CO_2 with photon energy requires materials that efficiently absorb light to generate electron–hole pairs with the eventual target of achieving a carbon-neutral artificial photosynthesis cycle by coupling the reductive half-reaction of CO_2 fixation with a matched oxidative half-reaction such as water oxidation. To achieve the photocatalytic reduction of CO_2 thermodynamically, the bottom of CB of photocatalysts should have a more negative potential than CO_2 reduction potentials, and the top of VB should be located at a more positive potential than the H_2O oxidation potential. The efficient performance of semiconductor photocatalysts should benefit from: i) the bandgap of semiconductors causes absorption of incident light to generate the electron–hole pairs across the region of solar spectrum; ii) electron–hole pairs separate effectively from each other and migrate to the surface; iii) photocatalysts provides enough quality and quantity of active sites such as adsorption sites and reaction centres, contributing to photocatalytic reaction. The overall efficiency of photocatalytic reduction of CO_2 is determined by the balance of thermodynamics and kinetics of the processes above.

In 1979, Inoue et al. initially reported photocatalytic reduction of CO_2 to organic compounds on various semiconductor photocatalysts suspended in CO_2 saturated water illuminated by

a Xe lamp, and different products have been obtained, such as CO, CH_4, CH_3OH, HCOOH or others.[4] Since photocatalysis is a surface/interface-reaction process, catalysts play an important role in development of useful transformations utilizing this attractive and environmentally friendly raw material. A series of characteristic properties of photocatalysts have a direct impact on the CO_2 conversion efficiency. So far, explored semiconductor materials for photocatalytic reduction of CO_2 include, but not limited to, metal oxides, metal sulfides, nitrides, and phosphides, as summarized in **Table 1**. Most metal oxides consist of metal cations with d^0 (Ti^{4+}, Zr^{4+}, Nb^{5+}, Ta^{5+}, V^{5+},Mo^{6+}, W^{+6}) and d^{10} (In^{3+}, Ga^{3+}, Ge^{4+}, Sn^{4+}, Sb^{5+}) configurations. The d^0 metal oxides contain titanates [TiO_2,[4,10,26,34–149] $ATiO_3$ (A = Sr, Ca, Ba, Pb),[150–154] $K_2Ti_6O_{13}$,[155,156] $ALa_4Ti_4O_{15}$ (A = Ca, Sr, Ba),[157] ZrO_2,[158–161] niobates [HNb_3O_8,[162,163] $InNbO_4$,[164] $ANbO_3$ (A = Li, Na, K),[165–169] tantalates [Ta_2O_5,[170,171] $InTaO_4$,[172–176] $ATaO_3$ (A = Li, Na, K),[177] vanadates ($BiVO_4$,[178] $Fe_2V_4O_{13}$[179] $Na_2V_6O_{16}$,[180] $Bi_6Mo_2O_{15}$,[181] and tungstates (WO_3,[182,183] $W_{18}O_{49}$,[184] Bi_2WO_6[185,186]. d^{10} metal oxides includes $In(OH)_3$,[187] gallates (Ga_2O_3,[188–190] $ZnGa_2O_4$,[191,192] $CuGaO_2$,[193] and germinates (Zn_2GeO_4,[194–197] $In_2Ge_2O_7$,[198] and stannates (Zn_2SnO_4.[199] Furthermore, d^{10} metal nitride solid solutions such as $(Zn_{1+x}Ge)(N_2O_x)$[200,201] and $(Ga_{1-x}Zn_x)(N_{1-x}O_x)$[202] were also found to be active. Metal sulfides such as CdS and ZnS,[4,203–214] MnS,[215] $Cu_xAg_yIn_zZn_kS$ solid solutions,[216] and Cu_2ZnSnS_4[217] have been applied for photocatalytic reduction of CO_2 in various solvents. The p-type silicon,[218–220] p-type InP[221–223] and p-GaP[224] as photocathodes have successfully achieved photo-electrochemical reduction of CO_2.

Although the study of the photocatalytic reduction of CO_2 started earlier, however, the CO_2 conversion efficiency still suffers from very low efficiencies. Fortunately, the design and engineering of photocatalysts with different architectures and surface properties have recently accelerated the development of novel and efficient photocatalyst, which involve bandgap engineering, nanostructuralization, surface oxygen vacancy engineering, macro/meso/microporous structuralization, exposure of highly active crystal facets, utilization of co-catalysts, and Z-scheme construction.

3.1. Band-Structure Engineering

Band-structure engineering is an effective approach to adjust bandgap and band position for utilizing solar energy effectively, and subsequently improve photoconversion efficiency of CO_2 reduction, involving quantum confinement effect, cation or anion doping, solid solution formation, hetero-structuralization and sensitization.

3.1.1. Quantum Confinement Effect

Quantum-confined semiconductor nanocrystals (NCs) have many ideal characteristics for light-harvesting and charge-separation applications.[225–227] Compared with molecular chromospheres,[228,229] NCs offer unique size-dependent absorption properties, large extinction coefficients over a broad spectral range, the possibility of generating multiple excitons by single photons, long exaction lifetimes, and enhanced photostability.[230] The surface of NCs can be readily modified for specific functional targets and/or reaction environments.[231] Higher yields of CH_3OH and CH_4 over the TiO_2 nanoparticles as the particle size decreased were detected under the illumination of light. The optimum particle size was a result of competing effects of specific surface area, charge–carrier dynamics, and light absorption efficiency.[82] Distinct from the bulk WO_3 for thermodynamically inactive CO_2 photoreduction, 4–5 nm thick WO_3 ultrathin nanosheets with dominant exposed {001} facets exhibited obvious performance for photocatalytic reduction of CO_2 into CH_4 under visible light irradiation, due to that size-quantization effects in vertical direction enlarges the WO_3 band gap.[182] The similar phenomenon was also observed for rectangular sheet-like WO_3 crystal with predominant {002} facet as photocatalyts for CO_2 reduction into CH_4.[183] Cd-rich CdSe nanocrystals below a certain critical size are efficient photocatalysts for CO_2 fixation in the presence of light, and bulk CdSe surfaces fail.[232,233] Small carbon nanoparticles of sub-10 nm in size harvest visible photons for subsequent charge separation on the particle surface to drive the efficient photocatalytic conversion of CO_2 into formic acid, which represents a highly promising new platform for visible-light photocatalysis of CO_2 conversion.[234]

3.1.2. Cation or Anion Doping

The potential of VB of most of currently developed metal oxide photocatalysts is normally located about 3 eV vs NHE,[235] which leads to that the metal oxide photocatalysts for CO_2 reduction only utilize the UV light. Replacing partial O in the metal oxides by anion such as N and C is a convenient strategy to raise VB maxima and narrow bandgap of metal oxides for efficiently widen the wavelength range of solar radiation that can be absorbed. N-doped mesoporous TiO_2 with Pt, Au, and Ag as co-catalysts absorbed light up to 500 nm in the visible light spectrum, which contributes to photocatalytic reduction of CO_2 under visible light irradiation ($\lambda > 420$ nm).[137] N-doped Ta_2O_5 linked with Ru complex electrocatalysts showed selective conversion of CO_2 to HCOOH under visible light irradiation ($410 < \lambda < 750$ nm).[170,171] N-doped $InTaO_4$ with Ni@NiO core shell nanostructure as co-catalyst displayed photocatalytic reduction of CO_2 with H_2O into CH_3OH under light irradiation ($390 < \lambda < 770$ nm).[176] I-doped TiO_2 exhibited activity for photocatalytic reduction of CO_2 with H_2O into CO under visible light irradiation ($\lambda > 400$ nm).[133] The p-n hybrid system of hollow CuO nanocubes decorated with nanoparticles of titanium oxynitride ($TiO_{2-x}N_x$) photocatalytically converted CO_2 into CH_4 at ambient temperature.[134]

Cations such as Cu,[95,130,140] Ni,[128,147] Ce,[130,146]and Ag[124,135] are usually doped into the lattice of TiO_2, creating impurity energy levels within the band gap. The behavior of charge carriers such as the recombination rate and interfacial electron-transfer rate is significantly influenced by the doping of cation.[236] Ce-doped TiO_2 enhanced photocatalytic activity for CO_2 reduction than pure TiO_2, mainly due to that the Ce^{3+}/Ce^{4+} redox couple facilitates electron–hole separation.[146] Ce atoms

Table 1. Summary of semiconductor-based systems on photocatalytic reduction of CO_2 (centralized from 1993 to 2013).[a)]

Light source	Catalyst	Co-catalyst	Reaction medium	Products	Efficiency	Reference (year)
UV Hg lamp (254 nm)	TiO_2 nanoparticles (4.5 to 29 nm)	–	CO_2-bubbled NaOH solution	CH_4,* CH_3OH	–	[82] (2009)
visible light $\lambda > 420$ nm	N-doped mesoporous TiO_2	Pt, Au, or Ag	CO_2 and H_2O vapor	CH_4	–	[137] (2012)
solar simulating light (AM1.5)	hybrid CuO-TiO_{2-x} N_x hollow nanocubes	–	CO_2 and H_2O vapor	CH_4,* C_2H_6, C_3H_8, C_4H_{10}	–	[137] (2012)
visible light $\lambda > 400$ nm	I-doped TiO_2 nanoparticles	–	CO_2 and H_2O vapor	CO	–	[133] (2011)
UV Xe lamp $250 < \lambda < 400$ nm	Cu-doped TiO_2 –SiO_2 mesoporous composite particles	–	CO_2 and H_2O vapor	CO	–	[95] (2011)
visible light $\lambda > 4$ 00 nm	Cu, I co-doped TiO_2 nanoparticles	–	CO_2 and H_2O vapor	CO,* CH_4	–	[145] (2012)
UV HgXe lamp	Cu, Ce co-doped TiO_2 nanoparticles	–	CO_2 bubbled solution	CH_3OH	QE = 26.5%	[140] (2012)
UV lamp (365nm)	Cu, Mn co-doped TiO_2 nanoparticles	–	CO_2 bubbled NaOH solution	CH_3OH	–	[130] (2011)
UV Xe lamp	Ce-doped TiO_2/SBA-15	–	CO_2 and H_2O vapor	CO,* CH_4	–	[146] (2012)
UV lamp (254 or 365 nm) or incandescent lamp (400–780 nm)	Ni, N co-doped TiO_2 nanoparticles	–	CO_2-bubbled NaOH solution containing Na_2SO_3	CH_3OH	–	[128] (2011)
Hg lamp (254 nm)	Ag-doped TiO_2 nanoparticles	–	CO_2 bubbled solution	CH_4,* CH_3OH	–	[124] (2010)
UV Hg lamp	rutile TiO_2 nanoparticle modified anatase TiO_2 nanorods	–	CO_2 and H_2O vapor	CH_4,* CH_3OH, H_2, CO	–	[105] (2012)
visible light $\lambda > 400$ nm	TiO_2 anatase–brookite junction	–	$NaHCO_3$ solution	CH_3OH	QE = 0.0717%	[141] (2012)
visible light $\lambda > 400$ nm	CdS(or Bi_2S_3)/TiO_2 nanotubes	–	CO_2-bubbled NaOH solution containing Na_2SO_3	CH_3OH	–	[136] (2012)
visible light $\lambda > 420$ nm	AgBr/TiO_2 nanocomposites	–	CO_2-saturated $KHCO_3$ solution containing NaOH	CH_4,* CH_3OH, C_2H_5OH, CO	–	[127] (2011)
concentrated natural sunlight	Fe and Cu co-doped TiO_2 sensitized with Ru dye	–	CO_2 and H_2O vapor	CH_4	–	[121] (2008)
visible light $\lambda > 420$ nm	enzyme-modified TiO_2 nanoparticles	–	CO_2 bubbled solution Containing MES	CO	–	[126] (2010)
visible light $\lambda > 420$ nm	copper(I) dye-sensitised TiO_2 nanoparticles	–	CO_2 and H_2O vapor	CH_4	–	[144] (2012)
tungsten–halogen lamp.	Cobalt-phthalocyanine (CoPc) dye/TiO_2	–	CO_2-bubbled NaOH solution containing Na_2SO_3	HCOOH,* CO, HCHO, CH_3OH ,CH_4	–	[118] (2007)
solar simulating light (AM1.5)	N-doped TiO_2 nanotube arrays	Cu and Pt	CO_2 and H_2O vapor	CH_4,* C_2H_4, C_2H_6	–	[83] (2009)
UV Xe lamp	TiO_2 rods with {010} facets	1 wt% Pt	CO_2 and H_2O vapor	CH_4	–	[91] (2011)
UV Xe lamp	1D TiO_2 film	Pt (1.04 nm)	CO_2 and H_2O vapor	CH_4,* CO	QE = 2.41%	[106] (2012)
solar simulating light (AM1.5)	TiO_2 nanotube arrays	$Cu_{0.33}$-$Pt_{0.67}$	CO_2 and H_2O vapor	CH_4,* C_2H_4, C_2H_6	–	[107] (2012)
UV Hg lamp	TS-1 zeolites	–	CO_2 and H_2	CH_4	–	[42] (1995)
UV Hg lamp	ex-Ti-oxide/Y-zeolite	1 wt% Pt	CO_2 and H_2O vapor	CH_4,* CH_3OH	–	[44] (1997)
UV Hg lamp	Ti-MCM-41 or Ti-MCM-48 zeolites	1 wt% Pt	CO_2 and H_2O vapor	CH_4,* CH_3OH	–	[48] (1998)
UV Hg lamp	Ti–β(F) or Ti–β(OH) zeolites	–	CO_2 and H_2O vapor	CH_4,* CH_3OH	–	[56] (2001)
UV Hg lamp	Titanium porous silica thin films	–	CO_2 and H_2O vapor	CH_4,* CH_3OH	QE = 0.28%	[60] (2002)
UV Hg lamp	Ti-SBA-15	–	CO_2 and H_2O vapor	CH_4,* CH_3OH	–	[70] (2005)

Table 1. Continued.

Light source	Catalyst	Co-catalyst	Reaction medium	Products	Efficiency	Reference (year)
UV lamp	Ti-KIT-6	–	CO_2 and H_2O vapor	CH_4	–	[109] (2013)
UV Xe lamp	porous silica supported TiO_2	0.5 wt% Cu	CO_2 and H_2O vapor	CO,* CH_4	QE = 1.41%	[86] (2010)
UV Xe lamp	Metal complex doped UiO-67 MOF	–	CO_2-saturated MeCN solution	CO,* H_2	–	[246] (2011)
visible light $420 < \lambda < 800$ nm	NH_2-MIL-125(Ti) MOF	–	CO_2-saturated MeCN/TEOA (5:1) solution	HCOOH	–	[247] (2012)
visible light $420 < \lambda < 800$ nm	NH_2-Uio-66(Zr) MOF	–	CO_2-saturated MeCN/TEOA (5:1) solution	HCOOH	–	[248] (2013)
UV Xe lamp	TiO_2/ZnO mesoporous "french fries"	–	CO_2 and H_2O vapor	CH_4	–	[96] (2011)
UV Xe lamp	hollow anatase TiO_2 single crystals with {101} facets	1 wt% RuO_2	CO_2 and H_2O vapor	CH_4	–	[100] (2012)
UV Xe lamp	TiO_2 ultrathin nanosheets with 95% of exposed {100} facet	–	CO_2 and H_2O vapor	CH_4	–	[113] (2013)
UV Xe lamp	P25	Pt@Cu_2O	CO_2 and H_2O vapor	CH_4,* CO, H_2	–	[114] (2013)
UV Hg lamp	TiO_2 nanoparticles	Pt or Pd	CO_2-bubbled solution	CH_4,* C_2H_6	–	[36] (1993)
UV Xe lamp	TiO_2 nanoparticles	Pd and RuO_2	CO_2-bubbled NaOH solution containing Na_2SO_3	HCOOH	–	[59] (2001)
UV Xe lamp	nafion coated Pd–TiO_2 particles	1.0 wt% Pd	CO_2-saturated Na_2CO_3 solution	CH_4,* C_2H_6	–	[101] (2012)
UV Hg lamp	TiO_2 nanoparticles	Cu	CO_2 and H_2O vapor	CH_3OH,* CH_4	–	[39] (1994)
UV lamp	TiO_2 nanoparticles	3.0 wt% CuO	CO_2-bubbled $KHCO_3$ aqueous solution	CH_3OH	QE = 19.23%	[116] (2005)
UV Hg lamp (254 nm)	TiO_2 nanoparticles	2.0 wt% Cu	CO_2-bubbled NaOH solution	CH_3OH, O_2	QE = 10%, η = 2.5%	[62(2002)
UV Hg lamp (365 nm)	TiO_2 coated on optical fiber	1.2 wt% Cu	CO_2 and H_2O vapor	CH_3OH	–	[73] (2005)
UV lamp	TiO_2 nanoparticles	0.03 wt% Cu	CO_2 and H_2O vapor	CH_4	–	[102] (2012)
UV Xe lamp	mesoporous TiO_2/graphitic carbon microspheres	–	CO_2 and H_2O vapor	CH_4	–	[115] (2013)
UV lamp (365 nm)	MWCNTs supported TiO_2	–	CO_2-saturated H_2O solution	HCOOH,* CH_4, C_2H_5OH	–	[77] (2007)
visible light $\lambda > 400$ nm	CNTs@Ni-doped TiO_2 nanocomposites	Ni	CO_2 and H_2O vapor	CH_4	–	[147] (2013)
UV Xe lamp	graphene-$Ti_{0.91}O_2$ hollow spheres	–	CO_2 and H_2O vapor	CO,* CH_4	–	[39] (2012)
UV Xe lamp	graphene-TiO_2 nanosheets	–	CO_2 and H_2O vapor	C_2H_6, CH_4	–	[111] (2013)
visible light $400 < \lambda < 850$ nm	less defective graphene-P25 nanocomposites	–	CO_2 and H_2O vapor	CH_4	–	[90] (2011)
visible light $\lambda > 400$ nm	self-doped $SrTiO_{3-\delta}$ particles	0.3%wt Pt	CO_2 and H_2O vapor	CH_4	E = 0.21%	[151] (2011)
UV Hg lamp	$SrTiO_3$ nanocrystals	7 wt% Ag	CO_2 bubbled CH_3OH solution	HCOOH	–	[152] (2012)
UV Xe lamp	leaf-architectured $SrTiO_3$	1 wt% Au	CO_2 and H_2O vapor	CO,* CH_4	–	[153] (2013)
UV Hg or Xe lamp	$K_2Ti_6O_{13}$ particles	Pt	CO_2-saturated H_2O solution	H_2,* CH_4, HCOOH, HCHO	–	[155] (2003)
UV Hg lamp	$BaLa_4Ti_4O_{15}$ nanoplates	Ag	CO_2 bubbled H_2O solution	CO,* HCOOH, H_2, O_2	–	[157] (2011)
UV Hg lamp	ZrO_2	1 wt% Cu	$NaHCO_3$ solution	CO	–	[158] (1993)
UV Xe lamp	SiO_2-Pillared HNb_3O_8	0.4 wt% Pt	CO_2 and H_2O vapor	CH_4	–	[162] (2012)
UV Xe lamp	HNb_3O_8 nanobelts	–	CO_2 and H_2O vapor	CH_4	–	[163] (2012)

REVIEW

Table 1. Continued.

Light source	Catalyst	Co-catalyst	Reaction medium	Products	Efficiency	Reference (year)
visible light 500 < λ < 900 nm	$InNbO_4$ (SSR)	1 wt% NiO	$KHCO_3$ aqueous solution	CH_3OH	–	[164] (2012)
UV Hg lamp	$LiNbO_3$ particles	–	CO_2-saturated H_2O solution	HCOOH,* HCHO	QE = 2%	[166] (2011)
UV Xe lamp	$NaNbO_3$ nanowires	Pt	CO_2 and H_2O vapor	CH_4	–	[165] (2011)
UV Xe lamp	cubic and orthorhombic $NaNbO_3$nanoparticles	Pt	CO_2 and H_2O vapor	CH_4	–	[167] (2012)
UV Xe lamp	$ANbO_3$ (A = Na, K) (SSR)	Pt	CO_2 and H_2O vapor	CH_4	–	[168] (2012)
visible light 410 < λ < 750 nm	N- DopedTa_2O_5	Ru-complex	CO_2-saturated MeCN/ TEOA (5:1) solution	HCOOH,* H_2, CO	QE = 1.9%	[170] (2010)
visible light 410 < λ < 750 nm	N- DopedTa_2O_5	Ru-complex	CO_2-saturated MeCN/ TEOA (5:1) solution	HCOOH,* CO	–	[171] (2011)
halogen lamp	$InTaO_4$ (SSR)	1 wt% NiO	$KHCO_3$ aqueous solution	CH_3OH	QE = 2.45%, η = 1.158%	[172] (2007)
halogen lamp 400 < λ < 1100 nm	$InTaO_4$ particles	1 wt% NiO	CO_2 bubbled NaOH solution	CH_3OH	QE = 0.063%	[174] (2010)
Xe lamp 390 < λ < 770 nm	N-doped $InTaO_4$ (SSR)	Ni@NiO core shell	CO_2 bubbled H_2O solution	CH_3OH	–	[176] (2011)
UV Hg–Xe lamp	$ATaO_3$ (A = Li, Na, K) (SSR)	–	CO_2 and H_2	CO	–	[177] (2010)
visible light λ > 400 nm	$BiVO_4$ monoclinic crystals	–	CO_2 bubbled H_2O solution	C_2H_5OH,* CH_3OH	–	[178] (2009)
visible light λ > 420 nm	$Fe_2V_4O_{13}$ nanoribbons	0.5 wt% Pt	CO_2 and H_2O vapor	CH_4	–	[179] (2013)
visible light λ > 420 nm	$Na_2V_6O_{16}$ nanoribbons	Pt and RuO_2	CO_2 and H_2O vapor	CH_4	–	[180] (2013)
UV Xe lamp	$Bi_6Mo_2O_{15}$ sub-microwires	–	CO_2 and H_2O vapor	CH_4, O_2	–	[181] (2013)
visible light λ > 420 nm	WO_3 nanosheets	–	CO_2 and H_2O vapor	CH_4	–	[182] (2012)
UV Xe lamp	rectangular sheet-like WO_3	–	CO_2 and H_2O vapor	CH_4	–	[183] (2012)
visible light λ > 420 nm	$W_{18}O_{49}$ nanowires	–	CO_2 and H_2O vapor	CH_4	–	[184] (2012)
visible light λ > 420 nm	Bi_2WO_6 nanoplates	–	CO_2 and H_2O vapor	CH_4	–	[185] (2012)
visible light λ > 420 nm	Bi_2WO_6 hollow microspheres	–	CO_2 bubbled H_2O solution	CH_3OH	–	[186] (2012)
UV Xe lamp	mesoporous $In(OH)_3$	0.5 wt% Pt	CO_2 and H_2O vapor	CH_4	–	[187] (2013)
UV Xe lamp	porous β-Ga_2O_3	–	CO_2 and H_2O vapor	CO,* CH_4	QE = 3.993%	[189] (2012)
UV Xe lamp	mesoporous $ZnGa_2O_4$	1 wt% RuO_2	CO_2 and H_2O vapor	CH_4	–	[191] (2010)
UV Xe lamp	$ZnGa_2O_4$ nanocubes	0.5 wt% RuO_2	CO_2 and H_2O vapor	CH_4, O_2	–	[192] (2012)
visible light λ > 420 nm	$ZnAl_2O_4$-modified mesoporous ZnGaNO	0.5 wt% Pt	CO_2 and H_2O vapor	CH_4	–	[202] (2012)
UV Xe lamp	$CuGaO_2$ (SSR)	–	CO_2 and H_2O vapor	CO,* CH_4	–	[193] (2012)
UV Xe lamp	Zn_2GeO_4 nanobelts	Pt, RuO_2	CO_2 and H_2O vapor	CH_4	–	[194] (2010)
UV Xe lamp	Zn_2GeO_4 nanorods	3 wt% RuO_2	CO_2 and H_2O vapor	CO,* CH_4	–	[195] (2011)
UV Xe lamp	mesoporous Zn_2GeO_4	1 wt% Pt	CO_2 and H_2O vapor	CH_4	QE = 0.2%	[196] (2011)
UV Xe lamp	ZIF-8/Zn_2GeO_4 nanorods	1 wt% Pt	CO_2 bubbled Na_2SO_3 solution	CH_3OH		[197] (2013)
visible light λ > 420 nm	sheaf-like, hyperbranched $Zn_{1.7}GeN_{1.8}O$	Pt and RuO_2	CO_2 and H_2O vapor	CH_4	QE = 0.024%	[200] (2012)
visible light λ > 400 nm	mesoporous $(Zn_{1+x}Ge)(N_2O_x)$	1 wt% Pt	CO_2 and H_2O vapor	CH_4,* CO	–	[201] (2012)
UV Xe lamp	4.5($ZnGa_2O_4$):(Zn_2GeO_4) solid solution	–	CO_2 and H_2O vapor	CH_4, O_2	–	[237] (2013)

Table 1. Continued.

Light source	Catalyst	Co-catalyst	Reaction medium	Products	Efficiency	Reference (year)
UV Xe lamp	$In_2Ge_2O_7$(En) nanowires	1 wt% Pt	CO_2 and H_2O vapor	CO, O_2	–	[198] (2012)
UV Xe lamp	Zn_2SnO_4 nanoplates	Pt and RuO_2	CO_2 and H_2O vapor	CH_4	–	[199] (2012)
UV Xe lamp	ZnS microcrystals	Cd	CO_2 bubbled 2-propanol solution	HCOOH,* H_2	QE = 32.5%	[205] (1995)
UV ($\lambda > 290$ nm)	ZnS nanoparticles supported on silica	–	CO_2 bubbled solution 2,5- containing DHF	HCOOH	–	[207] (1997)
UV ($\lambda > 290$ nm)	ZnS nanocrystals	–	CO_2 bubbled solution containing triethylamine	HCOOH,* CO, H_2	–	[209] (1998)
visible light $\lambda > 400$ nm	CdS nanocrystals	–	CO_2 bubbled solution containing triethylamine	CO	–	[206] (1997)
UV Hg-lamp	CdS nanocrystals	–	CO_2 bubbled solution	HCOOH,* HCHO	–	[208] (1998)
UV Hg-lamp	CdS particles	–	CO_2 bubbled 2-propanol solution	HCOOH,* CO, H_2	–	[210] (1998)
UV ($\lambda > 290$ nm)	CdS nanoparticles supported on silica	–	$NaHCO_3$ solution containing Na_2SO_3	HCOOH,* HCHO, oxalic acid	–	[211] (2002)
UV Hg-lamp (254 nm)	CdS nanoparticles deposited on montmorillonite	–	CO_2-saturated NaOH solutions	H_2,* CH_4, CO	–	[212] (2011)
visible light $\lambda > 420$ nm	enzyme coupled CdS nanocrystals	–	CO_2-saturated MES solution	CO	–	[213] (2012)
visible light $\lambda > 400$ nm	Bi_2S_3/CdS	–	CO_2-bubbled NaOH solution containing Na_2SO_3	CH_3OH	–	[214] (2011)
UV Hg lamp	MnS particles	–	$NaHCO_3$ solution containing NaHS	HCOOH,* CO	QE = 4.2%	[215] (2004)
visible light λ>400 nm	$Cu_xAg_yIn_zZn_kS$ solid solutions	RuO_2 or $Rh_{1.32}Cr_{0.66}O_3$	$NaHCO_3$ solution	CH_3OH	–	[216] (2011)
visible light $400 < \lambda < 800$ nm	Cu_2ZnSnS_4 photocathode	Ru-complex	CO_2-saturated solution	HCOOH	–	[217] (2011)
661 nm	p-Si photocathode	Re-complex	PEC cell	CO	$\eta = 9.3\%$	[218] (2010)
solar simulating light (AM1.5)	p-InP photocathode	Ru-complex	$NaHCO_3$ solution (PEC cell)	HCOOH,* O_2	$\eta = 0.04\%$	[222] (2011)
solar simulating light (AM1.5)	p-InP photocathode	Ru-complex	$NaHCO_3$ solution (PEC cell)	HCOOH,* O_2	$\eta = 0.14\%$	[223] (2013)
UV 365 nm	p-GaP photocathode	–	PEC cell	CH_3OH	$\eta = 9.3\%$, QE =44% at –0.5V	[224] (2008)
visible light $425 < \lambda < 720$ nm	carbon nanoparticles of sub-10 nm	Au	CO_2-saturated solution	HCOOH	–	[234] (2011)
UV Xe lamp	layered Zn-Al LDH	–	CO_2 and H_2	CO,* CH_3OH	–	[258] (2011)
UV Hg-Xe lamp	layered Mg-In LDH	–	CO_2-saturated H_2O solution	CO,* O_2	–	[259] (2012)
UV Xe lamp	layered Zn–Cu–Ga LDH	–	CO_2 and H_2	CH_3OH,* CO	–	[260] (2012)
visible light $\lambda > 420$ nm	g-C_3N_4	–	CO_2 and H_2O vapor	CO	–	[262] (2012)
visible light $\lambda > 420$ nm	mesoporous g-C_3N_4 flakes	–	CO_2-saturated NaOH solution	CH_3OH,* C_2H_5OH	QE = 0.18%	[263] (2013)
visible light $\lambda > 400$ nm	TaON–RuBLRu′	Ag	CO_2 bubbled MeOH solution	HCOOH,* H_2, CO	$\Delta G^\circ = +83.0$ kJ/mol	[267] (2013)

[a]The symbol '*'refers to the major product. 'SSR' refers to samples prepared by solid-state reaction. 'QE' refers to apparent quantum yield. 'η' refers to solar energy conversion efficiency. 'MWCNTs' and 'CNTs' refer to multiwalled carbon nanotubes and carbon nanotubes, respectively.

enter the crystal lattice of TiO_2 to bring lattice distortion and activate adsorbed H_2O and CO_2 molecules. Nevertheless, excessively high Ce concentration destroyed photocatalytic activity for CO_2 reduction as the formation of recombination centers by excess Ce accelerated electron–hole recombination, which was also observed in Cu-doped TiO_2.[95] Ce and Cu co-doped TiO_2 improved the efficiency for reduction of CO_2 into CH_3OH.[130] Ce doping affected the reaction more profoundly than that of Cu doping. Ag-doped TiO_2 (1–7 wt% Ag) caused the yield of CH_4 and CH_3OH by two mechanisms: up to 5wt% Ag doping in TiO_2 resulted in the shift of absorption edge towards visible light and increased generation of electron–hole pairs, and with Ag content above 5 wt%, the formation of Schottky barrier at the metal–semiconductor interface around Ag metallic clusters enhanced separation of electrons and holes.[124]

3.1.3. Solid Solutions

The solid solutions exhibit better performance than the single components comprising the solid solution. Solid solutions such as $(Ga_{1-x}Zn_x)(N_{1-x}O_x)$,[202] $(Zn_{1+x}Ge)(N_2O_x)$[200,201] and zinc gallogermanate solid solution[237] was utilized for photocatalytic reduction of CO_2. Yellow $Zn_{1.7}GeN_{1.8}O$ solid solution with a bandgap of 2.6 eV exhibited highest activity for CO_2 reduction with apparent quantum yield of 0.024% at wavelength of 420 ±15 nm when loading 1 wt% Pt and 1 wt% RuO_2 co-catalysts, originated from p-d repulsion of N2p and Zn3d orbitals which lifts the top of VB and then narrows the band gap.[200] Zinc gallogermanate (denoted as $(4.5(ZnGa_2O_4):(Zn_2GeO_4))$ solid solution that incorporates Zn_2GeO_4 into $ZnGa_2O_4$ can narrow band gap by the upshift of VB edge from the increased p-d (O2p-Zn3d) repulsion effect through incorporation of s and p orbitals of Ge, and the downshift of CB edge by introducing the low-energy orbital of Ge.[237] The zinc gallogermanate solid solution possesses a light-hole effective mass which is beneficial for improving hole mobility, and thus enhances the ability for water oxidation to provide protons for CO_2 reduction. $Cu_xAg_yIn_zZn_kS$ solid solutions (bandgap < 2 eV) customized with RuO_2 or $Rh_{1.32}Cr_{0.66}O_3$ co-catalyst showed high photocatalytic activity for reduction of CO_2 into CH_3OH under visible light irradiation.[216]

3.1.4. Heterostructures

Heterostructures consisting of two or more materials can optimize charge separation and photocatalytic properties by providing an additional control of the electron and hole wave functions in these materials (i.e., wave function engineering).[238] The heterostructures (type II) can promote the spatial separation of electron–hole pairs by transferring photoexcited electrons in the higher CB to the lower CB and holes in the lower VB to the higher VB (**Figure 4**a). Cu_2O/SiC,[239] Bi_2S_3/CdS,[214] and TiO_2/ZnO[96] heterostructures have been constructed for photocatalytic reduction of CO_2. Rutile TiO_2 nanoparticle modified anatase TiO_2 nanorods with exposed {010} facets showed higher photocatalytic reduction of CO_2 into CH_4 than pure anatase TiO_2 nanorods, due to the transfer of

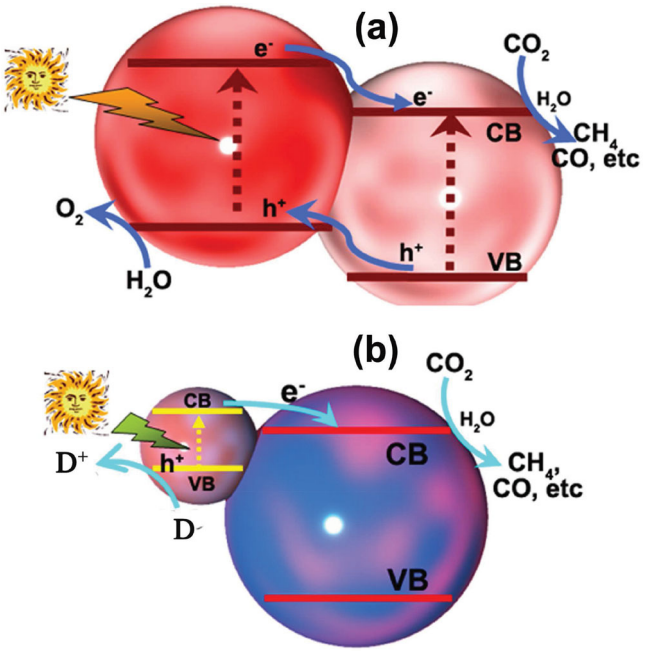

Figure 4. Schematic illustrations of: a) semiconductor heterostructures, b) sensitization of a wide band gap semiconductor with narrow-bandgap semiconductors or dye molecules for photocatalytic reduction of CO_2 with H_2O (D is a hole scavenger).

electrons from anatase to rutile under UV light irradiation.[105] Moreover, TiO_2 anatase–brookite junction exhibited remarkable photocatalytic performance for reduction of CO_2 into CH_3OH, resulting from the transfer of electrons from brookite to anatase.[141]

3.1.5. Sensitization

Sensitizing wide-bandgap semiconductors with narrow-bandgap semiconductors or dye molecules is an effective strategy to realize visible light reduction of CO_2 through the transfer of photogenerated electrons from narrow-bandgap semiconductors or dye molecules to the CB of wide-bandgap semiconductors (Figure 4b). Narrow-bandgap semiconductors such as CdS,[136] Bi_2S_3,[136] CdSe quantum dots (QDs),[125] PbS QDs,[131] and AgBr[127] have been coupled with TiO_2 for photocatalytic reduction of CO_2 under visible light irradiation. CdS or Bi_2S_3 sensitized TiO_2 nanotubes showed photocatalytic reduction of CO_2 into CH_3OH using Na_2SO_3 as a hole scavenger under visible light irradiation.[136] Photogenerated holes of $AgBr/TiO_2$ photocatalyst react with adsorbed H_2O molecules on the catalyst surface to form ·OH radicals and H^+ which take part in the formation of CH_4 and CH_3OH under visible light irradiation ($\lambda > 420$ nm).[127] The yields of CO, CH_4, and C_2H_6 over PbS QDs (3–5 nm) sensitized TiO_2 with Cu co-catalyst were also detected.[131]

Dye molecules have been linked with TiO_2 for photocatalytic reduction of CO_2 under visible light irradiation.[118–123,126,132,143,144,148] Compared with totally inactive pure TiO_2 under visible-light illumination, $[Ru(Bpy)_3]^{2+}$

dye-sensitized TiO_2 films showed efficient activity for reduction of CO_2 into CH_4, originating from transfer of the catalytically active electrons from organic dye to TiO_2.[119,120] Fe and Cu co-doped TiO_2 sensitized with Ru dye (N3 dye) were employed to reduce CO_2 with H_2O to CH_4 in an optical-fiber photoreactor under concentrated natural sunlight.[121] TiO_2 functionalized with the carbon monoxide dehydrogenases (CODHs) enzyme and a ruthenium bipyridyl sensitizer (RuP) was constructed for reduction of CO_2 into CO under visible light irradiation.[126,132] RuP injects electrons into the CB of TiO_2, and these electrons are transferred into CODH and the active sites where CO_2 is reduced to CO. TiO_2 with an air-stable copper (I) dye as a sensitizer exhibited efficient light harvesting and high efficiency for reduction of CO_2 into CH_4 under visible light irradiation ($\lambda > 420$ nm).[144] Cobalt-phthalocyanine (CoPc) dye[118,122,123] or zinc-phthalocyanine (ZnPc) dye[143] has been adsorbed on TiO_2 for CO_2 reduction under ambient conditions. CoPc-TiO_2 showed high selectivity for the formation of HCOOH while a small quantity of CO, HCHO, CH_3OH and CH_4 was generated in NaOH solution containing Na_2SO_3 as a hole scavenger.[118]

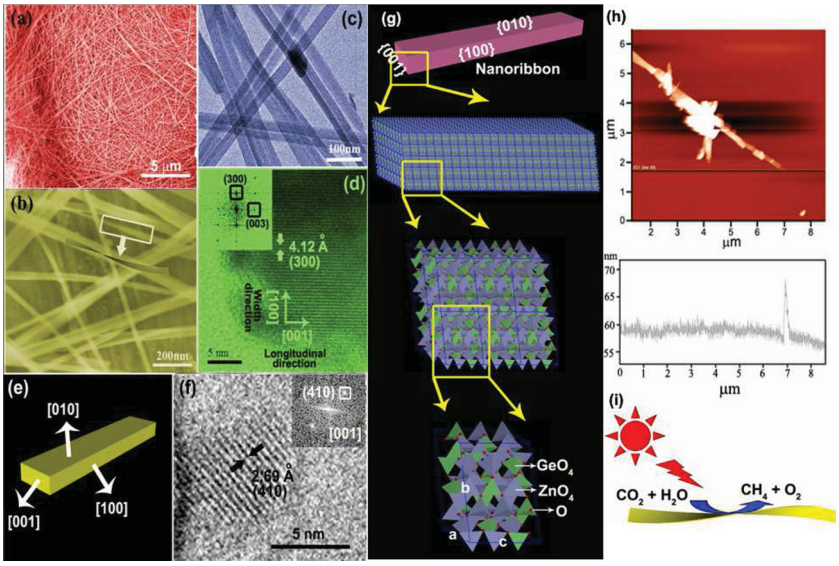

Figure 5. a,b) FE-SEM images, c) TEM and d) HRTEM images of Zn_2GeO_4 nanoribbon (the inset of (d) is the FFT pattern obtained from the HRTEM image); e) structural model of the nanoribbon, f) HRTEM image taken along [001], g) corresponding structural model of Zn_2GeO_4 nanoribbon, h) AFM image of Zn_2GeO_4 nanoribbon and corresponding high profile, and i) schematic illustration of photoreduction of CO_2 over the nanoribbon. Reproduced with permission.[194] Copyright 2010, American Chemical Society.

3.2. Nanostructuralization

Nanostructures in forms of nanorods, nanowires, nanotubes, nanobelts, etc have been extensively studied for photocatalytic application.[240,241] The nanostructured semiconductors are usually of single crystalline phases that exclude the possibility of any grain boundaries and defects in the materials (usually act as recombination sites in polycrystalline materials), which decreases the electron–hole recombination rate. Nanostructures, especially One-dimensional nanostructures, also provide a direct pathway for electron transport, which is favorable for improving the separation of electron–hole pairs.[242] Nanostructured semiconductors have proved to exhibit superior performance for photocatalytic reduction of CO_2 in recent years, such as TiO_2,[83,88,91,103,105–107,136] $Fe_2V_4O_{13}$ nanoribbons,[179] $Na_2V_6O_{16}$ nanoribbons,[180] HNb_3O_8 nanoribbons,[163] $NaNbO_3$ nanowires,[165] $In_2Ge_2O_7$(En) (En = ethylenediamine) hybrid sub-nanowires,[198] Zn_2GeO_4 nanoribbons and nanorods.[194,195,197]

Zn_2GeO_4 nanoribbons (ca. 7 nm thickness, corresponding to five repeating cell unit) with ultralong and ultrathin geometry greatly improved photocatalytic activity toward reduction of CO_2 with H_2O into CH_4 relative to bulk Zn_2GeO_4 (**Figure 5** and **6**).[194] The ultrathin geometry of the nanoribbons allows charge carriers to move rapidly from the interior to the surface to participate in the photoreduction reaction. The single crystalline hexagonal prism Zn_2GeO_4 nanorods (400 nm length and 50 nm width) also exhibited higher activity for photocatalytic reduction of CO_2 into CH_4.[195] $In_2Ge_2O_7$(En) ultrathin nanowire (2–3 nm in diameter) proved to possess photocatalytic activity towards the conversion of CO_2 to CO and O_2 in the present water vapor under Xe arc lamp irradiation.[198] $NaNbO_3$ nanowires with a uniform diameter of about 100 nm and length of up to several tens micrometers exhibited about 20-time significant improvement for photocatalytic reduction of CO_2 into CH_4 under UV–vis light irradiation, relative to bulk $NaNbO_3$, due to superior crystallinity, the high surface area, and highly mobile charge carriers.[165] 1D $Fe_2V_4O_{13}$ nanoribbon arrays with a bandgap of 1.83 eV directly grown on a stainless-steel mesh served as a new candidate for reduction of CO_2 into CH_4 under visible light irradiation.[179] This substrate-supported $Fe_2V_4O_{13}$ nanoribbons avoids the complex recycling process of powders from solution when photocatalytic reduction of CO_2 is carried in solution.

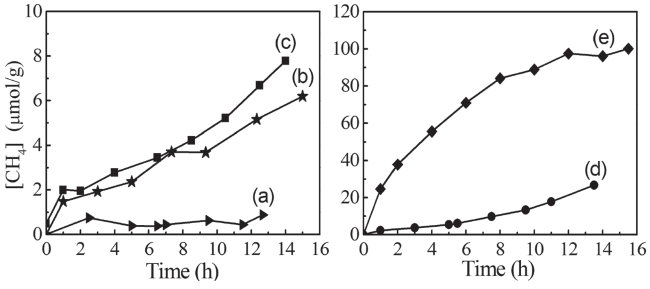

Figure 6. CH_4 generation over Zn_2GeO_4: solid-state reaction (a), nanoribbon (b), 1 wt% Pt-loaded nanoribbon (c), 1 wt% RuO_2-loaded nanoribbon (d), and 1 wt% RuO_2 and 1 wt% Pt co-loaded nanoribbons (e) as a function of light irradiation times. Reproduced with permission.[194] Copyright 2010, American Chemical Society.

3.3. Surface Oxygen Vacancy Engineering

Oxygen vacancy is an intrinsic defect in metal oxides, which is the most reactive site on the surface and able to modify the structure of the materials and change the electronic and chemical properties of the surface.[243] The surface oxygen vacancies sites of semiconductors play an important role in CO_2 activation[10,31,151,184,233,244,245] CO_2 molecules prefer to adsorb at oxygen vacancy sites with one oxygen atoms of the CO_2 located at bridging oxygen vacancy defects.[28,29] The attraction between an oxygen vacancy and a CO_2 molecule may lower the reactive barrier due to the generation of an unexpected affinity interaction. The combination of post-Hartree-Fock calculation and density-functional theory (DFT) calculation reveals that oxygen vacancy defects on TiO_2 surface is more effective for CO_2 activation than stoichiometric TiO_2 surface, due to stronger interaction between CO_2 and TiO_2.[31] A missing oxygen atom may leave two extra electrons at the site of the vacancy which reduce the adjacent two surface Ti^{4+} sites to Ti^{3+}, creating surface electron centers for the formation of the negatively charged $CO_2^{\bullet-}$ species, in which the overlap between the (C-O) π^* anti-bonding orbitals of CO_2 and Ti 3d orbitals is favorable for electron transfer into CO_2.

Oxygen-vacancy-rich ultrathin $W_{18}O_{49}$ nanowires showed an excellent capability of selective reduction of CO_2 into CH_4 under irradiation with visible light irradiation ($\lambda > 420$ nm).[184] The large number of oxygen vacancies existing in the nanowires, with a "trap" effect, can tightly "catch" CO_2 molecules and greatly enhance the adsorption of CO_2. Oxygen vacancies being fully consumed after irradiation for 90 h could be easily recovered by utilizing the strong reducing power of $NaBH_4$. Monoclinic phase $Bi_6Mo_2O_{15}$ microwires with post heating treatment at different temperatures from 600 °C to 800 °C showed increasing photocatalytic activity for reduction of CO_2 into CH_4, resulting from the increasing concentration of surface oxide vacancies with the increase of post heating treatment.[181] The surface oxide vacancies can greatly prolong lifetime of photoexcited carriers which be beneficial for the separation of electron–hole pairs. However, higher temperature treatment of $Bi_6Mo_2O_{15}$ at 900 °C led to the damage of photocatalytic activity, owing to the disorder of atom arrangement and the loss of the crystallinity. Similar phenomenon was also observed over self-doped $SrTiO_{3-\delta}$ with treatments in Ar at temperatures ranging from 1200 to 1400 °C for CO_2 reduction under visible light irradiation ($\lambda > 420$ nm), in which the oxygen vacancies and Ti^{3+} together induce an in-gap band to enhance the visible light absorption.[151] The sample treated at optimized temperature of 1300 °C realized the highest photocatalytic activity for CO_2 reduction with a quantum efficiency of 0.21% at 600 nm.

3.4. Macro-/Meso-/Microporous Structuralization

Porous materials usually have high surface areas, abundant surface states and readily accessed channels. Micro-/mesoporous photocatalysts for photocatalytic reduction of CO_2 are mainly classified two groups: i) photoactive species-dispersed zeolites,[42,44,48,51,52,56,57,63,70] mesoporous silica,[60,61,64,84,86,97,109,146] and metal–organic frameworks (MOFs);[197,246–248] and ii) pure mesoporous semiconductors, including TiO_2,[96,100,112,115,137] $In(OH)_3$,[187] Bi_2WO_6,[186] Ga_2O_3,[189] $ZnGa_2O_4$,[191,202,249] and Zn_2GeO_4.[196,201]

Zeolites are representative micro/mesoporous materials that have been widely modified with TiO_2 photocatalysts for CO_2 reduction by taking advantage of their high surface area, high pore volume, tunable pore size, and good thermal and mechanical stability.[250] The role of the siliceous zeolites can be described as a so-called "catch and release effect of CO_2", i.e., i) the condensation of the reactants within the hydrophobic cavities of zeolites and ii) the efficient diffusion of the reactant onto the TiO_2 active sites.[251] Ti-containing zeolites shows improved CO_2 adsorption, reactivity, and selectivity of the products, including TS-1,[42,51] Ti-oxide/Y-zeolite,[44,51] Ti-MCM-41,[48,51] Ti-MCM-48,[48,51] Ti-FSM-16 mesoporous zeolite,[52] and Ti–β zeolite.[56,57,63] The ex-Ti-oxide/Y-zeolite prepared by an ion-exchange method achieved a high photocatalytic efficiency and selectivity for the formation of CH_3OH in the photocatalytic reduction of CO_2 with H_2O, owing to that the titanium oxide species are highly dispersed within the zeolite cavities and exist in a tetrahedral coordination.[44] In contrast, CH_4 was major product using TiO_2 and imp-Ti-oxide/Y-zeolite as photocatalysts due to the involvement of aggregated octahedrally coordinated titanium oxide species. Compared with both Ti-MCM-41 with a large pore size (>20 Å) and 1D channel structure and TS-1 with smaller pore size (ca. 5.7 Å) and a three-dimensional (3D) channel structure, Ti-MCM-48 with a large pore size (>20 Å) and 3D channels showed higher photocatalytic efficiency and higher selectivity for the formation of CH_3OH, which is due to a combined contribution of the high dispersion state of the Ti-oxide species and large pore size with a 3D channel structure.[51]

The hydrophilic–hydrophobic properties of these zeolites also prove to be a controlling factor in the selectivity for photocatalytic reduction of CO_2 with H_2O.[56] Different concentrations of surface OH groups show different adsorption properties for H_2O molecules toward the catalyst surface. Two types of Ti–β zeolites by introducing OH^- and F^- ion during the prepared process possess hydrophilic and hydrophobic properties, respectively.[56] The selectivity for the formation of CH_3OH over Ti–β(F) with hydrophobic property was higher than that over Ti–β(OH) with hydrophilic property. A typical self-standing Ti-containing porous silica thin film with a hexagonal pore structure exhibited higher photocatalytic activity for reduction of CO_2 into CH_4 and CH_3OH with a high quantum yield of 0.28% than Ti-MCM-41 catalyst with the same pore structure in presence of water vapor under UV light irradiation.[60] Similar thin film with a cube pore structure and low concentration of surface OH groups showed higher selectivity for the formation of CH_3OH.[61]

SBA-15, one well-known mesoporous silica with 1D hexagonal pore, has been studied as a catalyst support for photocatalytic reduction of CO_2.[70,84,97,146] Ti-SBA-15 with an average pore diameter of 69 Å showed a 20-times increase of photocatalytic activity for reduction of CO_2 into CH_4 and CH_3OH in the presence of H_2O under UV light irradiation, compared with Ti-MCM-48 and Ti-MCM-41 with an average pore diameter of 27–29 Å, which was ascribed to higher dispersed titanium oxide species and larger pore size.[70] Ce-doped TiO_2 nanoparticles supported on SBA-15 mesoporous silica also remarkably enhanced photocatalytic activity for reduction of CO_2 into CO

and CH_4 under UV–vis illumination, relative to Ce–TiO_2, due to the more effective diffusion and adsorption of CO_2 through the ordered 1D pores in SBA-15.[146]

However, most of the reported zeolite and mespore-based photocatalysts already investigated are only active in the UV region and their efficiency for CO_2 reduction is still quite low. It is of great significance to develop highly efficient visible-light active photocatalysts. Metal–organic frameworks (MOFs) constructed by metal ions or small discrete clusters through the linkage of multidentate organic molecules are a new type of porous materials with crystalline frameworks.[252] The ability to organize different photoactive components in an MOF platform can make them comparable or even superior to the inorganic semiconductors to a certain degree to achieve artificial photosynthesis. The first MOF-based heterogeneous catalytic system was developed by doping different molecular complexes into Uio-67(Zr) for water oxidation, photocatalytic CO_2 reduction, and organic transformations under visible light irradiation, which highlights the potential of using functionalized MOFs as visible light-responsive photocatalysts for CO_2 reduction (**Figure 7**).[246] The introduction of NH_2 groups into Ti-based MOF $Ti_8O_8(OH)_4(bdc)_6$ (abbreviation as MIL-125(Ti)) to form $Ti_8O_8(OH)_4(bdc\text{-}NH_2)_6$ (NH_2-MIL-125(Ti)) allows extra absorption band in the visible light region with the absorption edge extending from 350 nm to around 550 nm, and an increase of adsorption capability toward CO_2.[247] The mechanism involves an electron transfer from the photoexcited organic ligand (visible-light-active 2-aminoterephthalate to the metal–oxo cluster $[TiO_5(OH)]$ in NH_2-MIL-125(Ti) to generate Ti^{III}, which is beneficial for the CO_2 reduction under visible light irradiation. NH_2-Uio-66(Zr) exhibited higher activity for CO_2 reduction than NH_2-MIL-125(Ti) in the presence of triethanolamine as sacrificial agent.[248] Zeolitic imidazolate frameworks (ZIFs), as a type of MOFs, have excellent thermal and chemical stability, and structural stability in water in addition to higher CO_2 adsorption properties than zeolites.[253] Zn_2GeO_4/ZIF-8 hybrid nanorods containing 25 wt% ZIF-8 exhibited 3.8-times higher dissolved CO_2 adsorption capacity than the bare Zn_2GeO_4 nanorods, resulting in a 62% enhancement in photocatalytic reduction of CO_2 into liquid CH_3OH fuel.[197]

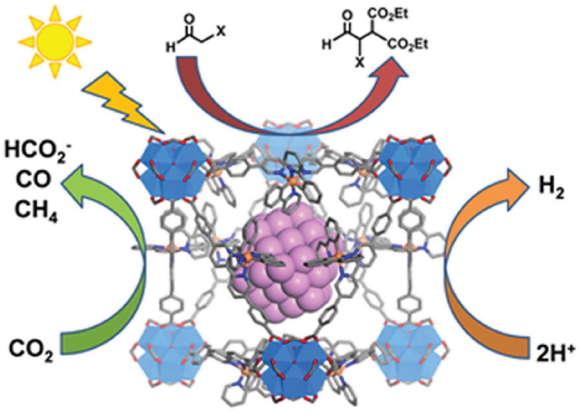

Figure 7. Schematic illustration of MOF-based heterogeneous catalytic system for water oxidation, photocatalytic CO_2 reduction, and organic transformations. Reproduced with permission.[246b] Copyright 2011, American Chemical Society.

In addition to the large surface area, pure mesoporous semiconductors have high degree of crystallinity that leads to effective separation and transport of electron–hole pairs, and subsequently favorable for improved photocatalytic performance for CO_2 reduction. A series of TiO_2-based mesoporous "french fries" (MFFs) (TiO_2/ZnO, TiO_2/Fe_2O_3, TiO_2/CuO, TiO_2/NiO, TiO_2/Cr_2O_3, and TiO_2/CeO_2) were obtained by a facile furfural alcohol-derived polymerization–oxidation route. The production rate of CO_2 to CH_4 generated in the hybrid TiO_2/ZnO MFFs is at least 56 times higher than those obtained in the solid state reaction (SSR)-TiO_2/ZnO and commercial P25, respectively. The high conversion efficiency results from: i) a faster diffusion transport of photogenerated electrons in hybrid TiO_2/ZnO than in pure TiO_2; ii) the reduced recombination rate of photogenerated electron–hole pairs; iii) a higher specific surface area, which provides more adsorption of CO_2 and H_2O vapor and more reaction active sites in the MFFs.[96] Mesoporous β-Ga_2O_3 with an average pore size of 3.8 nm realized enhanced photocatalytic activity for reduction of CO_2 into CO and CH_4 than commercial β-Ga_2O_3, due to higher surface area and mesoporous channels for efficient CO_2 adsorption.[189]

Mesoporous $ZnGa_2O_4$ with a wormhole framework by an ion-exchange reaction at room temperature with 1 wt% RuO_2 co-catalyst showed higher photocatalytic activity for reduction of CO_2 into CH_4 than $ZnGa_2O_4$ obtained by SSR-$ZnGa_2O_4$, owing to strong gas adsorption by the mesostructure and more reaction sites arising from high specific surface area (S_{BET} = 110.4 m^2 g^{-1} for meso-$ZnGa_2O_4$ and 4.6 m^2 g^{-1} for SSR-$ZnGa_2O_4$).[191] This ion-exchange method can be extended to prepare $ZnGa_2O_4$ nanocube[192] and other porous materials, such as $CoGa_2O_4$,[191] $NiGa_2O_4$,[191] Zn_2GeO_4[196,201] zinc gallogermanate solid solution,[237] and Bi_2WO_6.[186] Thus-prepared mesoporous Zn_2GeO_4 showed higher photocatalytic activity for reduction of CO_2 into CH_4 (9.5 ppm g^{-1} h^{-1}) compared with SSR-Zn_2GeO_4 (1.4 ppm g^{-1} h^{-1}).[196] The conversion efficiency could be further improved to 28.9 ppm g^{-1} h^{-1} with an apparent quantum yield of 0.2% at a wavelength of 251 ± 16 nm when loading with 1 wt% Pt co-catalyst. Mesoporous $(Zn_{1+x}Ge)(N_2O_x)$ by directly nitriding above mesoporous Zn_2GeO_4 at high temperature under an NH_3 atmosphere showed photocatalytic reduction of CO_2 into CH_4 under visible light irradiation ($\lambda > 400$ nm).[201] $ZnAl_2O_4$-modified mesoporous ZnGaNO solid solution synthesized by the combination of the ion-exchange method and nitriding treatment showed higher photocatalytic activity for CO_2 reduction than bulk ZnGaNO solid solution under visible light irradiation ($\lambda > 420$ nm), attributed to the following three reasons: i) Constructing mesoporous structure improves the gas adsorption; ii) $ZnAl_2O_4$ modification induces CO_2 chemisorbtion on the photocatalyst; iii) the high Zn content in the $ZnAl_2O_4$-modified ZnGaNO narrows the band gap and extends the light absorption.[202]

While micro/mesoporous photocatalysts significantly enhance gas-phase reaction efficiency, however, gas diffusion limitation has still been a concerning problem. Ye et al, utilized 3D unique hierarchical structures of a green leaf as architecture-directing agents to fabricate "meso/macro porous perovskite titanates ($ATiO_3$, A = Sr, Ca, Pb) 3D" towards CO_2 photoreduction.[153] This methology is desirable for development of a promising and ideal artificical photosynthesis system having

the analogous reaction features of natural photosynthesis by constructing: i) distinct 3D architecture for enhanced light harvesting; ii) efficient mass flow network of high surface areas and 3D multiple-scaled hierarchical porosity for suffering minimum gas diffusion and gas absorption; iii) appropriate catalysts with sufficiently negative CB for supplying strong reduction potential.

3.5. Crystal Facet Engineering

The surface atomic structure tunable by crystal facet engineering can adjust electronic band structure, surface energy and surface active sites, the adsorption of reactant, and desorption of reaction production.[254,255] Different surface structures have different selectivity for CO_2 adsorption and activation. Anatase TiO_2 is more favorable for CH_4 production, while rutile TiO_2 exhibits higher efficiency for the formation of CH_4 and CH_3OH.[40] Furthermore, the yield of CH_3OH formation over rutile TiO_2 was much higher on (100) than on (110), while the formation of CH_4 was only observed on (100) and but not on (110).[37] The reason is that (100) with a higher Ti/O surface ratio exhibits a more reductive property in the excited state than (110). Such a reductive surface allows a more facile reduction of CO_2 molecules especially for the formation of CH_4. Single crystalline anatase TiO_2 rods with dominant reactive {010} facets showed a superior photocatalytic conversion of CO_2 into CH_4 relative to benchmark P25 TiO_2 nanocrystals.[91] The interaction of CO_2 on the (010) is predicted stronger than on both (101) and (001).[256] The $ZnGa_2O_4$ nanocubes with exposed {100} facets exhibited improved performance in the photocatalytic reduction of CO_2 into CH_4 under UV–vis light irradiation, compared with mesporous $ZnGa_2O_4$ that has a larger specific surface area than $ZnGa_2O_4$ nanocubes.[192] The light-hole effective mass on the {100} facets of $ZnGa_2O_4$ nanocube corresponds to the high hole mobility, which contributes to the efficient H_2O oxidation to offer the protons for promoting CO_2 reduction into CH_4. The single crystal Zn_2GeO_4 nanorods with dominant (110) crystal face also exhibited improved photocatalytic activity for CO_2 reduction, owing to the high specific surface area and dominant (110) crystal face.[195] The exposure of the {001} crystalline facet of the well-defined Bi_2WO_6 nanoplate is a particular reactive surface energetically favoring the reduction of CO_2.[185] Monoclinic $BiVO_4$ is more efficient than tetragonal $BiVO_4$ for the photocatalytic reduction of CO_2 into ethanol in aqueous solution, due to a more efficient migration of photogenerated electrons from the V 3d-block bands to the anchored CO_2 on the surface monoclinic phase than tetragonal phase.[178] For the monoclinic phase, a more strong asymmetry in the local environment around the Bi^{3+} ion results in a stronger lone pair character in the Bi^{3+} ion and hence a stronger tendency to form a Bi–O bond with CO_2.[257]

It is interesting to note that sheet-like crystallites of molecular thickness and extremely high two-dimensional anisotropy can provide ratios of reactive sites on the surface that approach 100%. Recently, layered double hydroxides (LDHs) such as Zn-Al LDH,[258] Mg-In LDH,[259] and Zn–Cu–Ga LDH[258,260] are utilized for photocatalytic reduction of CO_2. The versatility of the LDH structure allows tuning the compositions of metal cations, charge balancing anions, and hydroxyl layer, which can adjust active sites, the adsorptive power of CO_2, and tolerance of water. However, their perseverance of photocatalytic reduction of CO_2 needs to be examined due to the poor chemical stability of LDH. g-C_3N_4 as a metal-free polymeric photocatalyst is considered as a promising visible-driven photocatalyst,[261] which has been applied for photocatalytic reduction for CO_2.[262,263]

3.6. Utilization of Co-catalysts

Co-catalysts are known to play crucial role in the semiconductor-based photocatalysis.[240] Firstly, co-catalysts can promote the separation and migration of photogenerated charge carriers to reduce the recombination of electron–hole pairs, resulting from the formation of Schottky barrier between semiconductor and co-catalyst. In the case of metal nanoparticles supported on the semiconductor including Pt,[44,83,88,106,114] Rh,[38,54] Pd,[34,36,59,93,98] Cu,[39,62,69,72,73,80,83,84,86,94,95,102,110,116] Ag[71,85,108,152,157] and Au,[137] the Fermi level of the metal normally lies below the CB edge of semiconductor, allowing the transfer of electrons from semiconductor to metal thermodynamically. Different valence states and particle size of co-catalysts influence the activity of photocatalytic reduction of CO_2. An optimal 3wt% CuO loaded TiO_2 showed higher activity for CO_2 reduction than TiO_2 with 3wt% Cu_2O or Cu, possibly due to lower potential redox of Cu^{2+}/Cu^{+} than that of Cu^{2+}/Cu^{0} or Cu^{+}/Cu^{0}.[116] Ultrafine Pt nanoparticles with optimized size of 0.5–2 nm promote TiO_2 films of 1D, single crystalline structure to display extremely high CO_2 photoreduction efficiency with highly selective formation of CH_4. Either smaller or bigger one resulted in lower performance.[106] The reason is that smaller Pt nanoparticles possibly have higher energy band separation due to quantum confinement, restraining electron transfer from the CB of TiO_2 to Pt. As Pt nanoparticles become larger, electrons can transfer freely to Pt nanoparticles with an energy level lower than −4.4 eV (the lower energy level of the CB of TiO_2). However, the properties of too large Pt nanoparticles may be approaching that of bulk Pt, capturing both photoelectrons and holes and acting as recombination centers. RuO_2 as oxidation site to collect holes is always loaded with other co-catalysts trapping electrons as reduction sites for photocatalytic reduction of CO_2.[59,194,200] The photocatalytic activity of reduction of CO_2 to $HCOO^-$ improved after RuO_2 and Pd were co-deposited on the surface of TiO_2, owing to that photogenerated electrons transfer from TiO_2 to Pd sites and photogenerated holes inject into RuO_2 sites.[59] Co-loading with 1 wt% Pt and 1 wt% RuO_2 on Zn_2GeO_4[194] or $Zn_{1.7}GeN_{1.8}O$[200] apparently enhanced photocatalytic activity for reduction of CO_2 into CH_4, even higher than the sum of the two individual co-catalysts, attributed to that Pt and RuO_2 can trap the electrons and holes respectively, hence inhibiting the recombination of electron–hole pairs.

Secondly, co-catalysts effectively lower the barrier for CO_2 activation, owing to their better conductivity and lower over potential. The activation energy of E_a for commercial P25 and 3wt% CuO loaded TiO_2 is ca. +26 and +12 kJ/mol, respectively.[116] The apparent lower activation energy of the latter hence improved the efficiency of CO_2 reduction. CO_2 on Rh-loaded TiO_2 prefers to bond to the surface with both C (linked

to a Rh atom) and one of the O atom (linked to the oxygen vacancy of TiO_2), which leads to the cleavage of C-O bond easily under light irradiation.[26a] The addition of MgO onto Pt-loaded TiO_2 significantly enhanced the activity of photocatalytic reduction of CO_2 to CH_4, because the chemisorbed CO_2 molecule on the MgO layer on TiO_2 crystallites becomes destabilized and its reactivity is believed to be higher than that of the linear CO_2 molecule.[26b]

Thirdly, co-catalysts can affect the selectivity of products in view of the formation of many different products during the process of CO_2 reduction. Deposition of a series of 2 wt% metals (Pt, Rh, Pd, Cu, Ru, and Au) on TiO_2 considerably accelerated photocatalytic reduction of CO_2 to CH_4 and/ or acetic acid, and product distribution could be controlled by changing sorts of the metals deposited on TiO_2.[36] Deposition of TiO_2 with Pt or Pd mainly produced CH_4, but a considerable amount of acetic acid was produced using other metals loaded TiO_2. NiO as an efficient co-catalyst was deposited on $InTaO_4$ with a bandgap of 2.6 eV for selective reduction of CO_2 into CH_3OH under visible light irradiation.[172,174,175]

Fourthly, the co-catalysts also play the role of inhibiting the back-recombination reaction,[241,264] including the re-oxidation (re-reduction) of hydrocarbon fuels (generated O_2) and the splitting of H_2O into H_2. Perovskite $BaLa_4Ti_4O_{15}$ plates with Ag co-catalyst on the edge exhibited high activity for photocatalytic reduction of CO_2 into CO, compared with pure $BaLa_4Ti_4O_{15}$ only for water splitting.[157] The reason is that the edge of a $BaLa_4Ti_4O_{15}$ photocatalyst is the reduction site while the basal plane is the oxidation site for water splitting. CO_2 reduction mainly proceeds on Ag co-catalyst loaded on the edge competing with H_2O reduction, while O_2 evolution mainly carries on the basal plane. The separation of the reaction sites could also contribute to suppression of back reactions such as oxidation of formed CO. Ni@NiO and similar core-shells such as $Rh@Cr_2O_3$ can prevent back reaction of the formation of H_2O from H_2 and O_2.[16] $Rh_{1.32}Cr_{0.66}O_3$ co-catalyst suppress the back reaction of reduction of O_2 to O_2^-, compared with $Cu_xAg_yIn_zZn_kS$ solid solutions with RuO_2 co-catalyst.[216]

The design of bifunctional co-catalysts with a proper structure is also crucial for obtaining high CO_2 conversion activity. A core–shell-structured $Pt@Cu_2O$ co-catalyst on TiO_2 was designed to promote photocatalytic reduction of CO_2 with H_2O to CH_4 and CO (**Figure 8**). The Pt core extracts the photogenerated electrons from TiO_2 and transfer the electrons to Cu_2O shell, and the Cu_2O shell provides sites for the preferential activation and conversion of CO_2.[114] Core-shell structure of metallic Ni core and NiO shell on the surface of $InTaO_4$ by reduction–oxidation pretreatment also exhibited a positive effect on the catalyst for improving activity for CO_2 reduction.[172] Ni core promotes the transfer of photogenerated electrons to NiO shell surface while NiO shell provides active sites to react with absorbed CO_2.[164,176] Cu_xPt_y alloy co-catalysts coated on N-doped TiO_2 nanotube arrays[83] or periodically modulated multiwalled TiO_2 nanotube arrays[107] showed exhibited high catalytic activity for the photoreduction of CO_2, in compared with individual Cu and Pt. The optimized $Cu_{0.33}Pt_{0.67}$ compositions were found to be the most reactive catalyst.[107]

Fifthly, in addition to acting as electron sinker (or trapper), the surface plasmon resonance mediated-photocatalysis of

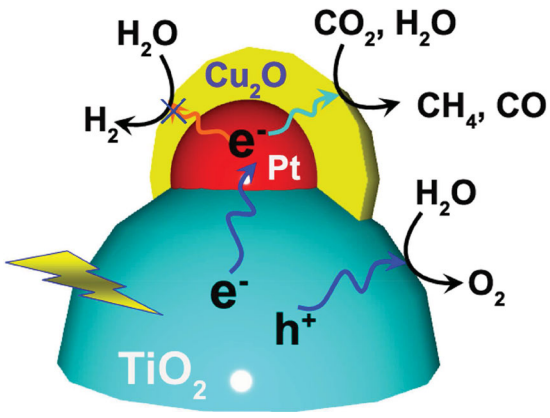

Figure 8. Schematic illustration of the $Pt@Cu_2O$ core-shell co-catalyst on TiO_2.

noble metals (mainly Ag and Au) becomes a rising research star in the harvesting conversion of solar energy (especially in visible region) recently.[129,265] Au-deposited TiO_2 film showed 24-times enhancement for CO_2 reduction in the presence of water vapor compared with pure TiO_2 under visible irradiation (532 nm), owing to the strong electric fields created by the surface plasmon resonance of the Au nanoparticles that excites electron–hole pairs locally in the TiO_2 at a rate several orders of magnitude higher than the normal incident light.[129] Additional products including CH_4, C_2H_6, CH_3OH, and HCHO were obtained under UV irradiation (254 nm), because the transfer of plasmon-excited electrons from Au to TiO_2 allows both the excited electrons in Au and TiO_2 contribute to CO_2 reduction with H_2O vapor.

Besides appropriate metals and metal oxides, carbon materials such as graphitic carbon,[115] carbon nanotube (CNT)[77,147] and graphene[90,104,111] can also act as electron acceptor and transporter to efficiently hinder recombination of electron–hole pairs, which play the role of co-catatlyst for photocatalytic reduction of CO_2. Anatase TiO_2 nanoparticles with diameter of 8–14 nm dispersed in the mesoporous graphitic carbon exhibited an excellent higher photocatalytic activity for reduction of CO_2 into CH_4 under simulated solar irradiation, compared with commercial P25.[115] CNT@Ni-doped TiO_2 showed higher activity for reduction of CO_2 into CH_4 than Ni-doped TiO_2 under visible light irradiation, mainly attributed to the transfer of electrons from TiO_2 to CNTs through d–p electron orbital overlap between TiO_2 and CNT.[147] Graphene offers an excellent electron-transport property and possesses an extremely high specific surface area for photocatalysis.[266] Robust hollow spheres consisting of $Ti_{0.91}O_2$ nanosheets and graphene showed 9-times enhancement for photocatalytic CO_2 reduction into dominant CO and minor CH_4 than commercial P25 (**Figure 9**), owing to: i) the ultrathin nature of $Ti_{0.91}O_2$ nanosheets could lead to rapid migration of charge carriers onto the surface for CO_2 reduction; ii) the compact stacking of both two-dimensional nanosheets through surface conjugation (d–π conjugate) enhances the lifetime of the charge carriers, due to the electron transfer from $Ti_{0.91}O_2$ nanosheets to graphene; iii) the hollow structure potentially acts as a photon trap to enhance light absorption by multiscattering of incidence

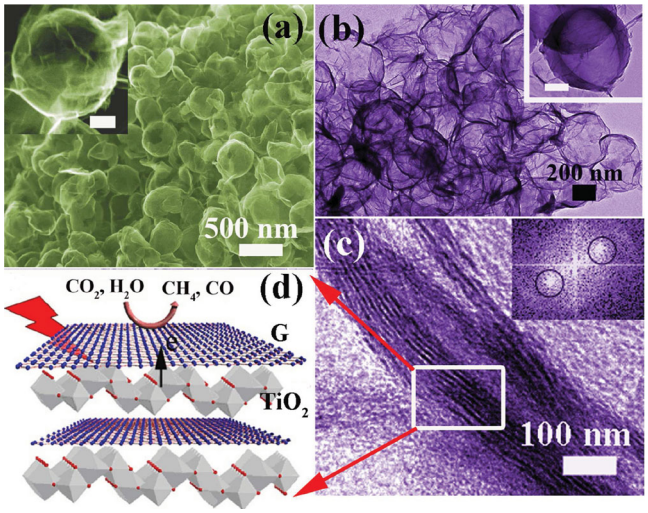

Figure 9. a) FE-SEM image and b,c) TEM image of $(G\text{-}Ti_{0.91}O_2)_5$ hollow spheres. d) Schematic illustration of alternating $Ti_{0.91}O_2$ nanosheets and G. Reproduced with permission.[104] Copyright 2012, Wiley-VCH.

light.[104] Graphene-TiO_2 hybrid nanosheets prepared by in situ simultaneous reduction-hydrolysis technique exhibited high and selective photocatalytic activity for CO_2 reduction into CH_4 and C_2H_6, which results from fast migration of electrons from TiO_2 to graphene promoted by the formation of d–π electron orbital overlap (Ti–O–C band).[111] The synergistic effect of the surface-Ti^{3+} sites and graphene is beneficial for the generation of C_2H_6, and the yield of the C_2H_6 increased with the content of incorporated graphene. Optimized graphene-P25 nanocomposites based on the less defective solvent-exfoliated graphene showed approximately 7-times improvement for reducing CO_2 into CH_4 than pure P25 under visible illumination.[90] The less-defective graphene, which possesses higher electrical mobility, facilitates the charge-carrier transport to surface sites to participate in the chemical reaction.

3.7. Z-Scheme Construction

The artificial Z-Scheme system, which imitates the natural photosynthesis of green plants for converting CO_2 into carbohydrates, was designed for photocatalytic reduction of CO_2 into hydrocarbon fuels.[222,223,267] The artificial Z-Scheme system consists of two different semiconductor photocatalysts with reversible redox mediators driven by a two-step photoexcitation, which has the merit of keeping electrons/holes with stronger reduction/oxidation abilities on different active sites (**Figure 10**). Arai et al. constructed a Z-scheme system for selective CO_2 conversion to $HCOO^-$ (formate) using a two-electrode configuration operated with no external electrical bias, which achieved a high selectivity for $HCOO^-$ production (>70%) and a solar energy conversion efficiency of 0.03–0.04% under simulated sunlight irradiation (AM1.5).[222] In the two-electrode configuration, p-type InP/Ru complex polymer hybrid photocatalyst for CO_2 reduction and TiO_2/Pt photocatalyst for H_2O oxidation were used as working electrode (photocathode) and counter electrode (photoanode), respectively. The enhancement

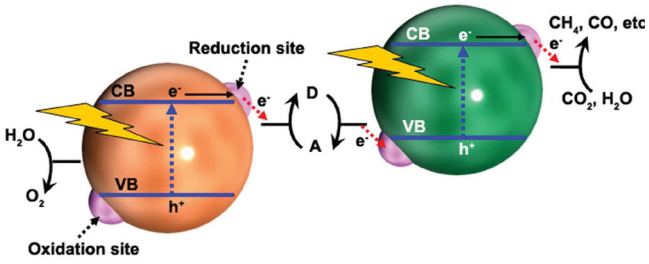

Figure 10. Schematic energy diagram of Z-scheme photocatalytic CO_2 reduction for a two-step photoexcitation system. D and A indicate electron donating and accepting species, respectively.

of conversion efficiency and reaction selectivity was mainly ascribed to the electron-transfer process from the photocathode to the photoanode. Furthermore, a higher solar energy conversion efficiency was achieved by substituting $SrTiO_3$ for TiO_2 as photoanode, ascribed to the more negative potential of the CB minimum of $SrTiO_3$ than TiO_2 to facilitate electron transfer from CB of the photoanode to VB of the photocathode.[223] Ishitani et al. successfully synthesized the first visible-light-driven Z-scheme for heterogeneous photocatalytic reduction of CO_2 under visible light irradiation ($\lambda > 400$ nm) by using a Ru(II) dinuclear complex (**RuBLRu′**) for CO_2 reduction and Ag-loaded TaON for methanol oxidation.[267] Isotope experiments clearly showed that this hybrid photocatalyst mainly produced HCOOH from CO_2 and HCHO from methanol, which could convert solar energy into chemical energy with a positive change in the Gibbs energy of 83.0 kJ mol^{-1}.

4. Challenges and Perspectives

The energy shortage and environmental related problems are becoming the worsening worldwide problems and the great challenges for human in the 21st century. The solar-driven reduction of CO_2 to value-added chemical fuels is a promising avenue to impact the global carbon balance, and the potential rewards are enormous. The present goal is to synthesize photoactive materials able to chemically couple these light driven redox reactions together and achieve conversion efficiency and selectivity that exceeds Nature's photosynthesis. However, photoconversion of CO_2 involves thermodynamically uphill, multielectron, multihole and multiproton processes occurring on a multicomponent photocatalyst. Longstanding challenges are presented in the fields of catalysis, energy science, semiconductor physics and engineering, and green chemistry.

To develop effective CO_2 fixation and conversion, several key considerations must be balanced, including: i) a deep understanding of processes that occur on the surface of photocatalysts during CO_2 reduction, e.g., adsorption/desorption of CO_2 and intermediate products, as well as the role of adsorbed water. In this regard, the research would integrate experimental and computational approaches to evaluate catalyst activity toward CO_2 photoreduction, and would advance fundamental understanding in the multidisciplinary areas of material science, surface chemistry, photocatalysis, and nanotechnology. Scanning tunneling microscopy (STM) would directly determine CO_2 adsorption sites and probe molecular orbitals

and charge transfer. Density functional theory (DFT) calculations of the local density of states, lowest-energy molecular structure, and vibrational modes would theoretically clarify potential reaction mechanisms. The synergy of STM and DFT would provide a logical framework for future study aimed at building an atomic-scale understanding of CO_2 photoreduction; ii) potential great improvement of efficiency in CO_2 photoreduction can result from significantly increasing the lifetime of the charge-separated state. The time scale of this electron–hole recombination is two to three orders of magnitude faster than other electron-transfer processes. Therefore, any process that inhibits electron–hole recombination would greatly increase the efficiency and rates of CO_2 photoreduction. For example, electrical conductivity and diffusion length of the photocatalyst should be as high as possible to minimize recombination of electron–hole pairs. Ultrathin nanostructures may also facilitate the charge-carrier transport to surface reaction sites to participate reductive chemistry. Spatial separation of photoexcited electrons and holes can also be reduced the electron–hole recombination, which was achieved by co-catalysts, Z-scheme or heterostuctures of coupling two semiconductors with properly aligned band structructs; iii) the kinetics of CO_2 photoreduction is also dependent upon light absorption by the photocatalyst. Many optical techniques are potentially useful for harvesting light for improvement of the efficiency including: structuring for multiple light scattering to increase the effective optical path length, and up-conversion to transform non-absorbed infrared light to absorbed visible light; iv) high surface area and porosity are required to maximize the adsorption, transport and desorption of reactants, intermediates and products; v) as defects such as oxygen vacancies control most of the chemistry at many metal oxide surfaces, oxygen vacancies is believed to act as a very important role on electron trapping and activating CO_2. The oxygen vacancies can be created either by doping with other anions or cations or by thermal treatments of stoichiometric photocatalysts, and these defects can be detected with in situ electron paramagnetic resonance spectroscopy, ultraviolet photoemission spectroscopy, and metastable impact electron spectroscopy and so on; vi) a high-efficiency process is also necessary to be founded on photoactive materials made of earth abundant, nontoxic, light-stable, scalable and low cost materials.

In addition, the efficiency of photocatalytic reduction of CO_2 could be deactivated after irradiation for long time. The deactivating phenomenon in the photocatalytic reduction of CO_2 can be attributed to the following three reasons: i) the adsorption or accumulation of intermediate products on the semiconductor surface could occupy photocatalytic reaction centers and also hinder the adsorption of CO_2 or H_2O, which could lead the deactivation of semiconductors under the continuous irradiation; ii) the desorption of hydrocarbon production affects the continuous adsorption of reactants that take part in the photocatalytic reaction; iii) the surface contamination of semiconductors shields the light absorption, resulting in the reduction of the generation of electron–hole pairs. Therefore, it is necessary to pay more attention on the study of semiconductor deactivation in future work.

Nobel Laureate Jean Marie Lehn said "If it exists it can be synthesized". To learn nature's photosynthesis, which generates everything "under the sun", it is sincerely hoped that multiple collaboration for this rapidly evolving field can lead to a breakthrough in the overall efficiency for the industrialization and commercialization with cost competitive with fossil fuels.

Acknowledgements

This work was supported by the 973 Programs (No. 2014CB239302, 2011CB933303, and 2013CB632404), the National Science Foundation of Jiangsu Province (No. BK2012015 and BK 20130053), the National Natural Science Foundation of China (No. 51272101), and the College Postgraduate Research and Innovation Project of Jiangsu Province (No. CXZZ13_0033).

Received: January 7, 2014
Revised: March 7, 2014
Published online: May 26, 2014

[1] A. J. Bard, M. A. Fox, *Acc. Chem. Res.* **1995**, *28*, 141.
[2] M. Aresta, A. Dibenedetto, *Dalton. Trans.* **2007**, 2975.
[3] M. Halmann, *Nature* **1978**, *275*, 115.
[4] T. Inoue, A. Fujishima, S. Konishi, K. Honda, *Nature* **1979**, *277*, 637.
[5] A. Pichon, *Energy Materials: A Stretch to Save the World* **2010**, http://www.natureasia.com/en/nchina/article/10.1038/nchina.2010.126.
[6] H. Yoneyama, *Catal. Today.* **1997**, *39*, 169.
[7] P. Usubharatana, D. McMartin, A. Veawab, P. Tontiwachwuthikul, *Ind. Eng. Chem. Res.* **2006**, *45*, 2558.
[8] G. R. Dey, *J. Nat. Gas Chem.* **2007**, *16*, 217.
[9] K. Koci, L. Obalova, Z. Lacny, *Chem. Pap.* **2008**, *62*, 1.
[10] V. P. Indrakanti, J. D. Kubicki, H. H. Schobert, *Energy Environ. Sci.* **2009**, *2*, 745.
[11] S. C. Roy, O. K. Varghese, M. Paulose, C. A. Grimes, *ACS Nano* **2010**, *4*, 1259.
[12] M. R. Hoffmann, J. A. Moss, M. M. Baum, *Dalton Trans.* **2011**, *40*, 5151.
[13] A. Dhakshinamoorthy, S. Navalon, A. Corma, H. Garcia, *Energy Environ. Sci.* **2012**, *5*, 9217.
[14] G. H. Liu, N. Hoivik, K. Y. Wang, H. Jakobsen, *Sol. Energy Mater Sol. Cells* **2012**, *105*, 53.
[15] K. Mori, H. Yamashita, M. Anpo, *RSC Adv.* **2012**, *2*, 3165.
[16] W. Q. Fan, Q. H. Zhang, Y. Wang, *Phys. Chem. Chem. Phys.* **2013**, *15*, 2632.
[17] S. N. Habisreutinger, L. Schmidt-Mende, J. K. Stolarczyk, *Angew. Chem. Int. Ed.* **2013**, *52*, 7372.
[18] Y. Izumi, *Coord. Chem. Rev.* **2013**, *257*, 171.
[19] V. Jeyalakshmi, K. Rajalakshmi, R. Mahalakshmy, K. R. Krishnamurthy, B. Viswanathan, *Res. Chem. Intermed.* **2013**, *39*, 2565.
[20] S. Navalon, A. Dhakshinamoorthy, M. Alvaro, H. Garcia, *ChemSusChem* **2013**, *6*, 562.
[21] D. G. Nocera, *Acc. Chem. Res.* **2012**, *45*, 767.
[22] A. L. Linsebigler, G. Q. Lu, J. T. Yates, *Chem. Rev.* **1995**, *95*, 735.
[23] A. J. Morris, G. J. Meyer, E. Fujita, *Acc. Chem. Res.* **2009**, *42*, 1983.
[24] K. Tanaka, D. Ooyama, *Coord. Chem. Rev.* **2002**, *226*, 211.
[25] L. Liu, W. L. Fan, X. Zhao, H. G. Sun, P. Li, L. M. Sun, *Langmuir* **2012**, *28*, 10415.
[26] a) J. Rasko, F. Solymosi, *J. Phys. Chem.* **1994**, *98*, 7147; b) S. Xie, Y. Wang, Q. Zhang, W. Fan, W. Deng, Y. Wang, *Chem. Commun.* **2013**, *49*, 2451.

[27] N. M. Dimitrijevic, B. K. Vijayan, O. G. Poluektov, T. Rajh, K. A. Gray, H. Y. He, P. Zapol, *J. Am. Chem. Soc.* **2011**, *133*, 3964.
[28] J. Lee, D. C. Sorescu, X. Y. Deng, *J. Am. Chem. Soc.* **2011**, *133*, 10066.
[29] S. J. Tan, Y. Zhao, J. Zhao, Z. Wang, C. X. Ma, A. D. Zhao, B. Wang, Y. Luo, J. L. Yang, J. G. Hou, *Phys. Rev. B.* **2011**, *84*.
[30] W. H. Koppenol, J. D. Rush, *J. Phys. Chem.* **1987**, *91*, 4429.
[31] V. P. Indrakanti, H. H. Schobert, J. D. Kubicki, *Energy Fuels* **2009**, *23*, 5247.
[32] H. J. Freund, M. W. Roberts, *Surf. Sci. Rep.* **1996**, *25*, 225.
[33] C. J. Gagliardi, B. C. Westlake, C. A. Kent, J. J. Paul, J. M. Papanikolas, T. J. Meyer, *Coord. Chem. Rev.* **2010**, *254*, 2459.
[34] Z. Goren, I. Willner, A. J. Nelson, A. J. Frank, *J. Phys. Chem.* **1990**, *94*, 3784.
[35] M. Anpo, K. Chiba, *J. Mol. Catal.* **1992**, *74*, 207.
[36] O. Ishitani, C. Inoue, Y. Suzuki, T. Ibusuki, *J. Photochem. Photobiol. A.* **1993**, *72*, 269.
[37] H. Inoue, T. Matsuyama, B. J. Liu, T. Sakata, H. Mori, H. Yoneyama, *Chem. Lett.* **1994**, 653.
[38] F. Solymosi, I. Tombacz, *Catal. Lett.* **1994**, *27*, 61.
[39] H. Yamashita, H. Nishiguchi, N. Kamada, M. Anpo, Y. Teraoka, H. Hatano, S. Ehara, K. Kikui, L. Palmisano, A. Sclafani, M. Schiavello, M. A. Fox, *Res. Chem. Intermed.* **1994**, *20*, 815.
[40] M. Anpo, H. Yamashita, Y. Ichihashi, S. Ehara, *J. Electroanal. Chem.* **1995**, *396*, 21.
[41] F. Saladin, L. Forss, I. Kamber, *J. Chem. Soc., Chem. Commun.* **1995**, 533.
[42] S. Yamagata, M. Nishijo, N. Murao, S. Ohta, I. Mizoguchi, *Zeolites* **1995**, *15*, 490.
[43] T. Mizuno, K. Adachi, K. Ohta, A. Saji, *J. Photochem. Photobiol. A.* **1996**, *98*, 87.
[44] M. Anpo, H. Yamashita, Y. Ichihashi, Y. Fujii, M. Honda, *J. Phys. Chem. B* **1997**, *101*, 2632.
[45] S. Kaneco, H. Kurimoto, K. Ohta, T. Mizuno, A. Saji, *J. Photochem. Photobiol. A.* **1997**, *109*, 59.
[46] B. J. Liu, T. Torimoto, H. Matsumoto, H. Yoneyama, *J. Photochem. Photobiol. A.* **1997**, *108*, 187.
[47] F. Saladin, I. Alxneit, *J. Chem. Soc., Faraday Trans.* **1997**, *93*, 4159.
[48] M. Anpo, H. Yamashita, K. Ikeue, Y. Fujii, S. G. Zhang, Y. Ichihashi, D. R. Park, Y. Suzuki, K. Koyano, T. Tatsumi, *Catal. Today.* **1998**, *44*, 327.
[49] S. Kaneco, Y. Shimizu, K. Ohta, T. Mizuno, *J. Photochem. Photobiol. A.* **1998**, *115*, 223.
[50] B. J. Liu, T. Torimoto, H. Yoneyama, *J. Photochem. Photobiol. A.* **1998**, *115*, 227.
[51] H. Yamashita, Y. Fujii, Y. Ichihashi, S. G. Zhang, K. Ikeue, D. R. Park, K. Koyano, T. Tatsumi, M. Anpo, *Catal. Today.* **1998**, *45*, 221.
[52] K. Ikeue, H. Yamashita, M. Anpo, *Chem. Lett.* **1999**, 1135.
[53] S. Kaneco, H. Kurimoto, Y. Shimizu, K. Ohta, T. Mizuno, *Energy* **1999**, *24*, 21.
[54] Y. Kohno, H. Hayashi, S. Takenaka, T. Tanaka, T. Funabiki, S. Yoshida, *J. Photochem. Photobiol. A.* **1999**, *126*, 117.
[55] M. Subrahmanyam, S. Kaneco, N. Alonso-Vante, *Appl. Catal., B* **1999**, *23*, 169.
[56] K. Ikeue, H. Yamashita, M. Anpo, T. Takewaki, *J. Phys. Chem. B* **2001**, *105*, 8350.
[57] K. Ikeue, H. Yamashita, T. Takewaki, M. E. Davis, M. Anpo, *J. Synchrotron. Radiat.* **2001**, *8*, 602.
[58] Y. Kohno, T. Yamamoto, T. Tanaka, T. Funabiki, *J. Mol. Catal. A: Chem.* **2001**, *175*, 173.
[59] T. F. Xie, D. J. Wang, L. J. Zhu, T. J. Li, Y. J. Xu, *Mater. Chem. Phys.* **2001**, *70*, 103.
[60] K. Ikeue, S. Nozaki, M. Ogawa, M. Anpo, *Catal. Lett.* **2002**, *80*, 111.
[61] I. Keita, S. Nozaki, M. Ogawa, M. Anpo, *Catal. Today.* **2002**, *74*, 241.
[62] I. H. Tseng, W. C. Chang, J. C. S. Wu, *Appl. Catal., B* **2002**, *37*, 37.
[63] H. Yamashita, K. Ikeue, T. Takewaki, M. Anpo, *Top. Catal.* **2002**, *18*, 95.
[64] Y. Shioya, K. Ikeue, M. Ogawa, M. Anpo, *Appl. Catal., A* **2003**, *254*, 251.
[65] G. R. Dey, A. D. Belapurkar, K. Kishore, *J. Photochem. Photobiol. A.* **2004**, *163*, 503.
[66] Y. Ku, W. H. Lee, W. Y. Wang, *J. Mol. Catal. A: Chem.* **2004**, *212*, 191.
[67] P. Pathak, M. J. Meziani, Y. Li, L. T. Cureton, Y. P. Sun, *Chem. Commun.* **2004**, 1234.
[68] I. H. Tseng, J. C. S. Wu, *Catal. Today.* **2004**, *97*, 113.
[69] I. H. Tseng, J. C. S. Wu, H. Y. Chou, *J. Catal.* **2004**, *221*, 432.
[70] J. S. Hwang, J. S. Chang, S. E. Park, K. Ikeue, M. Anpo, *Top. Catal.* **2005**, *35*, 311.
[71] P. Pathak, M. J. Meziani, L. Castillo, Y. P. Sun, *Green. Chem.* **2005**, *7*, 667.
[72] J. C. S. Wu, H. M. Lin, *Int. J. Photoenergy.* **2005**, *7*, 115.
[73] J. C. S. Wu, H.-M. Lin, C.-L. Lai, *Appl. Catal., A* **2005**, *296*, 194.
[74] Y. Q. Liu, Y. Xu, Z. J. Li, X. P. Zhang, D. Wu, Y. H. Sun, *Acta. Chim. Sinica* **2006**, *64*, 453.
[75] G. R. Dey, K. K. Pushpa, *Res. Chem. Intermed.* **2007**, *33*, 631.
[76] C.-C. Lo, C.-H. Hung, C.-S. Yuan, J.-F. Wu, *Sol. Energy Mater. Sol Cells* **2007**, *91*, 1765.
[77] X. H. Xia, Z. H. Jia, Y. Yu, Y. Liang, Z. Wang, L. L. Ma, *Carbon* **2007**, *45*, 717.
[78] T. V. Nguyen, J. C. S. Wu, *Sol. Energy Mater. Sol Cells* **2008**, *92*, 864.
[79] T.-V. Nguyen, J. C. S. Wu, *Appl. Catal., A* **2008**, *335*, 112.
[80] J. C. S. Wu, T. H. Wu, T. C. Chu, H. J. Huang, D. P. Tsai, *Top. Catal.* **2008**, *47*, 131.
[81] L. Chen, M. E. Graham, G. H. Li, D. R. Gentner, N. M. Dimitrijevic, K. A. Gray, *Thin. Solid. Films.* **2009**, *517*, 5641.
[82] K. Koci, L. Obalova, L. Matejova, D. Placha, Z. Lacny, J. Jirkovsky, O. Solcova, *Appl. Catal., B* **2009**, *89*, 494.
[83] O. K. Varghese, M. Paulose, T. J. LaTempa, C. A. Grimes, *Nano. Lett.* **2009**, *9*, 731.
[84] H. C. Yang, H. Y. Lin, Y. S. Chien, J. C. S. Wu, H. H. Wu, *Catal. Lett.* **2009**, *131*, 381.
[85] L. F. Cueto, G. T. Martinez, G. Zavala, E. M. Sanchez, *J. Nano. Res.* **2010**, *9*, 89.
[86] Y. Li, W. N. Wang, Z. L. Zhan, M. H. Woo, C. Y. Wu, P. Biswas, *Appl. Catal., B* **2010**, *100*, 386.
[87] K. Nalepa, J. Goralski, M. I. Szynkowska, J. Rynkowski, *Przem. Chem.* **2010**, *89*, 500.
[88] X. Feng, J. D. Sloppy, T. J. LaTempa, M. Paulose, S. Komarneni, N. Bao, C. A. Grimes, *J. Mater. Chem.* **2011**, *21*, 13429.
[89] K. Koci, V. Matejka, P. Kovar, Z. Lacny, L. Obalova, *Catal. Today.* **2011**, *161*, 105.
[90] Y. T. Liang, B. K. Vijayan, K. A. Gray, M. C. Hersam, *Nano. Lett.* **2011**, *11*, 2865.
[91] J. Pan, X. Wu, L. Z. Wang, G. Liu, G. Q. Lub, H. M. Cheng, *Chem. Commun.* **2011**, *47*, 8361.
[92] S. Y. Qin, F. Xin, Y. D. Liu, X. H. Yin, W. Ma, *J. Colloid. Interface Sci.* **2011**, *356*, 257.
[93] K. S. Raja, Y. R. Smith, N. Kondamudi, A. Manivannan, M. Misra, V. Subramanian, *Electrochem. Solid State Lett.* **2011**, *14*, F5.
[94] B. Srinivas, B. Shubhamangala, K. Lalitha, P. A. K. Reddy, V. D. Kumari, M. Subrahmanyam, B. R. De, *Photochem. Photobiol.* **2011**, *87*, 995.
[95] W.-N. Wang, J. Park, P. Biswas, *Catal. Sci. Technol.* **2011**, *1*, 593.
[96] G. C. Xi, S. X. Ouyang, J. H. Ye, *Chem. Eur. J.* **2011**, *17*, 9057.
[97] C. C. Yang, J. Vernimmen, V. Meynen, P. Cool, G. Mul, *J. Catal.* **2011**, *284*, 1.

[98] T. Yui, A. Kan, C. Saitoh, K. Koike, T. Ibusuki, O. Ishitani, *ACS Appl. Mater. Interfaces* **2011**, *3*, 2594.
[99] A. Cybula, M. Klein, A. Zielinska-Jurek, M. Janczarek, A. Zaleska, *Physicochem. Probl. Miner. Process.* **2012**, *48*, 159.
[100] W. Jiao, L. Z. Wang, G. Liu, G. Q. Lu, H. M. Cheng, *ACS Catal* **2012**, *2*, 1854.
[101] W. Kim, T. Seok, W. Choi, *Energy Environ. Sci.* **2012**, *5*, 6066.
[102] D. Liu, Y. Fernandez, O. Ola, S. Mackintosh, M. Maroto-Valer, C. M. A. Parlett, A. F. Lee, J. C. S. Wu, *Catal. Commun.* **2012**, *25*, 78.
[103] J. Z. Y. Tan, Y. Fernandez, D. Liu, M. Maroto-Valer, J. C. Bian, X. W. Zhang, *Chem. Phys. Lett.* **2012**, *531*, 149.
[104] W. G. Tu, Y. Zhou, Q. Liu, Z. P. Tian, J. Gao, X. Y. Chen, H. T. Zhang, J. G. Liu, Z. G. Zou, *Adv. Funct. Mater.* **2012**, *22*, 1215.
[105] P. Q. Wang, Y. Bai, J. Y. Liu, Z. Fan, Y. Q. Hu, *Catal. Commun.* **2012**, *29*, 185.
[106] W. N. Wang, W. J. An, B. Ramalingam, S. Mukherjee, D. M. Niedzwiedzki, S. Gangopadhyay, P. Biswas, *J. Am. Chem. Soc.* **2012**, *134*, 11276.
[107] X. J. Zhang, F. Han, B. Shi, S. Farsinezhad, G. P. Dechaine, K. Shankar, *Angew. Chem. Int. Ed.* **2012**, *51*, 12732.
[108] C. Y. Zhao, A. Kroll, H. L. Zhao, Q. Y. Zhang, Y. Li, *Int. J. Hydrogen. Energy* **2012**, *37*, 9967.
[109] M. Hussain, P. Akhter, N. Russo, G. Saracco, *Catal. Commun.* **2013**, *36*, 58.
[110] L. Liu, F. Gao, H. Zhao, Y. Li, *Appl. Catal., B* **2013**, *134–135*, 349.
[111] W. G. Tu, Y. Zhou, Q. Liu, S. C. Yan, S. S. Bao, X. Y. Wang, M. Xiao, Z. G. Zou, *Adv. Funct. Mater.* **2013**, *23*, 1743.
[112] Y. G. Wang, B. Li, C. L. Zhang, L. F. Cui, S. F. Kang, X. Li, L. H. Zhou, *Appl. Catal., B* **2013**, *130*, 277.
[113] H. Xu, S. X. Ouyang, P. Li, T. Kako, J. H. Ye, *ACS Appl. Mater. Interfaces* **2013**, *5*, 1348.
[114] Q. G. Zhai, S. J. Xie, W. Q. Fan, Q. H. Zhang, Y. Wang, W. P. Deng, Y. Wang, *Angew. Chem. Int. Ed.* **2013**, *52*, 5776.
[115] C. L. Zhang, Q. Y. Zhang, S. F. Kang, B. Li, X. Li, Y. G. Wang, *ECS Solid State Lett.* **2013**, *2*, M49.
[116] Slamet, H. W. Nasution, E. Purnama, S. Kosela, J. Gunlazuardi, *Catal. Commun.* **2005**, *6*, 313.
[117] N. Sasirekha, S. J. S. Basha, K. Shanthi, *Appl. Catal., B* **2006**, *62*, 169.
[118] S. H. Liu, Z. H. Zhao, Z. Z. Wang, *Photochem. Photobiol. Sci.* **2007**, *6*, 695.
[119] O. Ozcan, F. Yukruk, E. U. Akkaya, D. Uner, *Top. Catal.* **2007**, *44*, 523.
[120] O. Ozcan, F. Yukruk, E. U. Akkaya, D. Uner, *Appl. Catal., B* **2007**, *71*, 291.
[121] T. V. Nguyen, J. C. S. Wu, C. H. Chiou, *Catal. Commun.* **2008**, *9*, 2073.
[122] Z. H. Zhao, J. M. Fan, S. H. Liu, Z. Z. Wang, *Chem. Eng. J.* **2009**, *151*, 134.
[123] Z. H. Zhao, J. M. Fan, M. M. Xie, Z. Z. Wang, *J. Cleaner Prod.* **2009**, *17*, 1025.
[124] K. Koci, K. Mateju, L. Obalova, S. Krejcikova, Z. Lacny, D. Placha, L. Capek, A. Hospodkova, O. Solcova, *Appl. Catal., B* **2010**, *96*, 239.
[125] C. J. Wang, R. L. Thompson, J. Baltrus, C. Matranga, *J. Phys. Chem. Lett.* **2010**, *1*, 48.
[126] T. W. Woolerton, S. Sheard, E. Reisner, E. Pierce, S. W. Ragsdale, F. A. Armstrong, *J. Am. Chem. Soc.* **2010**, *132*, 2132.
[127] M. Abou Asi, C. He, M. H. Su, D. H. Xia, L. Lin, H. Q. Deng, Y. Xiong, R. L. Qiu, X. Z. Li, *Catal. Today.* **2011**, *175*, 256.
[128] J. Fan, E. Z. Liu, L. Tian, X. Y. Hu, Q. He, T. Sun, *J. Environ. Eng. Am. Soc. Civ. Eng.* **2011**, *137*, 171.
[129] W. B. Hou, W. H. Hung, P. Pavaskar, A. Goeppert, M. Aykol, S. B. Cronin, *ACS Catal.* **2011**, *1*, 929.
[130] D. M. Luo, Y. Bi, W. Kan, N. Zhang, S. G. Hong, *J. Mol. Struct.* **2011**, *994*, 325.
[131] C. J. Wang, R. L. Thompson, P. Ohodnicki, J. Baltrus, C. Matranga, *J. Mater. Chem.* **2011**, *21*, 13452.
[132] T. W. Woolerton, S. Sheard, E. Pierce, S. W. Ragsdale, F. A. Armstrong, *Energy Environ. Sci.* **2011**, *4*, 2393.
[133] Q. Y. Zhang, Y. Li, E. A. Ackerman, M. Gajdardziska-Josifovska, H. L. Li, *Appl. Catal., A* **2011**, *400*, 195.
[134] S.-I. In, D. D. Vaughn, R. E. Schaak, *Angew. Chem. Int. Ed.* **2012**, *51*, 3915.
[135] S. Krejcikova, L. Matejova, K. Koci, L. Obalova, Z. Matej, L. Capek, O. Solcova, *Appl. Catal., B* **2012**, *111*, 119.
[136] X. Li, H. L. Liu, D. L. Luo, J. T. Li, Y. Huang, H. L. Li, Y. P. Fang, Y. H. Xu, L. Zhu, *Chem. Eng. J.* **2012**, *180*, 151.
[137] X. K. Li, Z. J. Zhuang, W. Li, H. Q. Pan, *Appl. Catal., A* **2012**, *429*, 31.
[138] L. J. Liu, C. Y. Zhao, Y. Li, *J. Phys. Chem. C* **2012**, *116*, 7904.
[139] L. J. Liu, H. L. Zhao, J. M. Andino, Y. Li, *ACS Catal* **2012**, *2*, 1817.
[140] P. L. Richardson, M. L. N. Perdigoto, W. Wang, R. J. G. Lopes, *Appl. Catal., B* **2012**, *126*, 200.
[141] Q. D. Truong, T. H. Le, J. Y. Liu, C. C. Chung, Y. C. Ling, *Appl. Catal., A* **2012**, *437*, 28.
[142] Q. D. Truong, J. Y. Liu, C. C. Chung, Y. C. Ling, *Catal. Commun.* **2012**, *19*, 85.
[143] Q. Wang, W. Wu, J. F. Chen, G. W. Chu, K. Ma, H. K. Zou, *Colloids Surfaces A.* **2012**, *409*, 118.
[144] Y. J. Yuan, Z. T. Yu, J. Y. Zhang, Z. G. Zou, *Dalton Trans.* **2012**, *41*, 9594.
[145] Q. Y. Zhang, T. T. Gao, J. M. Andino, Y. Li, *Appl. Catal., B* **2012**, *123*, 257.
[146] C. Y. Zhao, L. J. Liu, Q. Y. Zhang, J. Wang, Y. Li, *Catal. Sci. Technol.* **2012**, *2*, 2558.
[147] W. J. Ong, M. M. Gui, S. P. Chai, A. R. Mohamed, *RSC Adv* **2013**, *3*, 4505.
[148] G. Qin, Y. Zhang, X. Ke, X. Tong, Z. Sun, M. Liang, S. Xue, *Appl. Catal., B* **2013**, *129*, 599.
[149] P. L. Richardson, M. L. N. Perdigoto, W. Wang, R. J. G. Lopes, *Appl. Catal., B* **2013**, *132–133*, 408.
[150] J. C. Hemminger, R. Carr, G. A. Somorjai, *Chem. Phys. Lett.* **1978**, *57*, 100.
[151] K. Xie, N. Umezawa, N. Zhang, P. Reunchan, Y. Zhang, J. Ye, *Energy Environ. Sci.* **2011**, *4*, 4211.
[152] D. D. Sui, X. H. Yin, H. Z. Dong, S. Y. Qin, J. S. Chen, W. L. Jiang, *Catal. Lett.* **2012**, *142*, 1202.
[153] H. Zhou, J. J. Guo, P. Li, T. X. Fan, D. Zhang, J. H. Ye, *Sci. Rep.* **2013**, *3*.
[154] M. Ulman, B. Aurianblajeni, M. Halmann, *Israel. J. Chem.* **1982**, *22*, 177.
[155] G. Q. Guan, T. Kida, T. Harada, M. Isayama, A. Yoshida, *Appl. Catal., A* **2003**, *249*, 11.
[156] G. Q. Guan, T. Kida, A. Yoshida, *Appl. Catal., B* **2003**, *41*, 387.
[157] K. Iizuka, T. Wato, Y. Miseki, K. Saito, A. Kudo, *J. Am. Chem. Soc.* **2011**, *133*, 20863.
[158] K. Sayama, H. Arakawa, *J. Phys. Chem.* **1993**, *97*, 531.
[159] Y. Kohno, T. Tanaka, T. Funabiki, S. Yoshida, *Chem. Commun.* **1997**, 841.
[160] Y. Kohno, T. Tanaka, T. Funabiki, S. Yoshida, *J. Chem. Soc., Faraday Trans.* **1998**, *94*, 1875.
[161] Y. Kohno, T. Tanaka, T. Funabiki, S. Yoshida, *Phys. Chem. Chem. Phys.* **2000**, *2*, 2635.
[162] X. K. Li, W. Li, Z. J. Zhuang, Y. S. Zhong, Q. Li, L. Y. Wang, *J. Phys. Chem. C* **2012**, *116*, 16047.
[163] X. K. Li, H. Q. Pan, W. Li, Z. J. Zhuang, *Appl. Catal., A* **2012**, *413*, 103.
[164] D. S. Lee, H. J. Chen, Y. W. Chen, *J. Phys. Chem. Solids.* **2012**, *73*, 661.

[165] H. F. Shi, T. Z. Wang, J. Chen, C. Zhu, J. H. Ye, Z. G. Zou, *Catal. Lett.* **2011**, *141*, 525.
[166] M. Stock, S. Dunn, *Ferroelectrics* **2011**, *419*, 9.
[167] P. Li, S. X. Ouyang, G. C. Xi, T. Kako, J. H. Ye, *J. Phys. Chem. C* **2012**, *116*, 7621.
[168] H. Shi, Z. Zou, *J. Phys. Chem. Solids.* **2012**, *73*, 788.
[169] P. Li, S. X. Ouyang, Y. J. Zhang, T. Kako, J. H. Ye, *J. Mater. Chem. A.* **2013**, *1*, 1185.
[170] S. Sato, T. Morikawa, S. Saeki, T. Kajino, T. Motohiro, *Angew. Chem. Int. Ed.* **2010**, *49*, 5101.
[171] T. M. Suzuki, H. Tanaka, T. Morikawa, M. Iwaki, S. Sato, S. Saeki, M. Inoue, T. Kajino, T. Motohiro, *Chem. Commun.* **2011**, *47*, 8673.
[172] P. W. Pan, Y. W. Chen, *Catal. Commun.* **2007**, *8*, 1546.
[173] H. C. Chen, H. C. Chou, J. C. S. Wu, H. Y. Lin, *J. Mater. Res.* **2008**, *23*, 1364.
[174] Z.-Y. Wang, H.-C. Chou, J. C. S. Wu, D. P. Tsai, G. Mul, *Appl. Catal., A* **2010**, *380*, 172.
[175] P. Y. Liou, S. C. Chen, J. C. S. Wu, D. Liu, S. Mackintosh, M. Maroto-Valer, R. Linforth, *Energy Environ. Sci.* **2011**, *4*, 1487.
[176] C. W. Tsai, H. M. Chen, R. S. Liu, K. Asakura, T. S. Chan, *J. Phys. Chem. C* **2011**, *115*, 10180.
[177] K. Teramura, S.-i. Okuoka, H. Tsuneoka, T. Shishido, T. Tanaka, *Appl. Catal., B* **2010**, *96*, 565.
[178] Y. Y. Liu, B. B. Huang, Y. Dai, X. Y. Zhang, X. Y. Qin, M. H. Jiang, M. H. Whangbo, *Catal. Commun.* **2009**, *11*, 210.
[179] P. Li, Y. Zhou, W. G. Tu, Q. Liu, S. C. Yan, Z. G. Zou, *ChemPlusChem* **2013**, *78*, 274.
[180] S. Feng, X. Chen, Y. Zhou, W. Tu, P. Li, H. Li, Z. Zou, *Nanoscale* **2014**, *6*, 1896.
[181] P. Li, Y. Zhou, W. G. Tu, R. Wang, C. F. Zhang, Q. Liu, H. J. Li, Z. D. Li, H. Dai, J. J. Wang, S. C. Yan, Z. G. Zou, *CrystEngComm* **2013**, *15*, 9855.
[182] X. Y. Chen, Y. Zhou, Q. Liu, Z. D. Li, J. G. Liu, Z. G. Zou, *ACS Appl. Mater. Interfaces* **2012**, *4*, 3372.
[183] Y. P. Xie, G. Liu, L. C. Yin, H. M. Cheng, *J. Mater. Chem.* **2012**, *22*, 6746.
[184] G. C. Xi, S. X. Ouyang, P. Li, J. H. Ye, Q. Ma, N. Su, H. Bai, C. Wang, *Angew. Chem. Int. Ed.* **2012**, *51*, 2395.
[185] Y. Zhou, Z. P. Tian, Z. Y. Zhao, Q. Liu, J. H. Kou, X. Y. Chen, J. Gao, S. C. Yan, Z. G. Zou, *ACS Appl. Mater. Interfaces* **2011**, *3*, 3594.
[186] H. F. Cheng, B. B. Huang, Y. Y. Liu, Z. Y. Wang, X. Y. Qin, X. Y. Zhang, Y. Dai, *Chem. Commun.* **2012**, *48*, 9729.
[187] J. J. Guo, S. X. Ouyang, T. Kako, J. H. Ye, *Appl. Surf. Sci.* **2013**, *280*, 418.
[188] H. Tsuneoka, K. Teramura, T. Shishido, T. Tanaka, *J. Phys. Chem. C* **2010**, *114*, 8892.
[189] H. A. Park, J. H. Choi, K. M. Choi, D. K. Lee, J. K. Kang, *J. Mater. Chem.* **2012**, *22*, 5304.
[190] K. Teramura, H. Tsuneoka, T. Shishido, T. Tanaka, *Chem. Phys. Lett.* **2008**, *467*, 191.
[191] S. C. Yan, S. X. Ouyang, J. Gao, M. Yang, J. Y. Feng, X. X. Fan, L. J. Wan, Z. S. Li, J. H. Ye, Y. Zhou, Z. G. Zou, *Angew. Chem. Int. Ed.* **2010**, *49*, 6400.
[192] S. C. Yan, J. J. Wang, H. L. Gao, N. Y. Wang, H. Yu, Z. S. Li, Y. Zhou, Z. G. Zou, *Adv. Funct. Mater.* **2013**, *23*, 758.
[193] J. W. Lekse, M. K. Underwood, J. P. Lewis, C. Matranga, *J. Phys. Chem. C* **2012**, *116*, 1865.
[194] Q. Liu, Y. Zhou, J. H. Kou, X. Y. Chen, Z. P. Tian, J. Gao, S. C. Yan, Z. G. Zou, *J. Am. Chem. Soc.* **2010**, *132*, 14385.
[195] S. C. Yan, L. J. Wan, Z. S. Li, Z. G. Zou, *Chem. Commun.* **2011**, *47*, 5632.
[196] N. Zhang, S. X. Ouyang, P. Li, Y. J. Zhang, G. C. Xi, T. Kako, J. H. Ye, *Chem. Commun.* **2011**, *47*, 2041.
[197] Q. Liu, Z. X. Low, L. X. Li, A. Razmjou, K. Wang, J. F. Yao, H. T. Wang, *J. Mater. Chem. A.* **2013**, *1*, 11563.
[198] Q. Liu, Y. Zhou, Y. Ma, Z. G. Zou, *RSC Adv.* **2012**, *2*, 3247.
[199] Z. D. Li, Y. Zhou, J. Y. Zhang, W. G. Tu, Q. Liu, T. Yu, Z. G. Zou, *Cryst. Growth. Des.* **2012**, *12*, 1476.
[200] Q. Liu, Y. Zhou, Z. P. Tian, X. Y. Chen, J. Gao, Z. G. Zou, *J. Mater. Chem.* **2012**, *22*, 2033.
[201] N. Zhang, S. X. Ouyang, T. Kako, J. H. Ye, *Chem. Commun.* **2012**, *48*, 1269.
[202] S. Yan, H. Yu, N. Wang, Z. Li, Z. Zou, *Chem. Commun.* **2012**, *48*, 1048.
[203] B. R. Eggins, J. T. S. Irvine, E. P. Murphy, J. Grimshaw, *J. Chem. Soc., Chem. Commun.* **1988**, 1123.
[204] M. Kanemoto, T. Shiragami, C. J. Pac, S. Yanagida, *J. Phys. Chem.* **1992**, *96*, 3521.
[205] H. Inoue, H. Moriwaki, K. Maeda, H. Yoneyama, *J. Photochem. Photobiol. A.* **1995**, *86*, 191.
[206] H. Fujiwara, H. Hosokawa, K. Murakoshi, Y. Wada, S. Yanagida, T. Okada, H. Kobayashi, *J. Phys. Chem. B* **1997**, *101*, 8270.
[207] P. Johne, H. Kisch, *J. Photochem. Photobiol. A.* **1997**, *111*, 223.
[208] B. R. Eggins, P. K. J. Robertson, E. P. Murphy, E. Woods, J. T. S. Irvine, *J. Photochem. Photobiol. A.* **1998**, *118*, 31.
[209] H. Fujiwara, H. Hosokawa, K. Murakoshi, Y. Wada, S. Yanagida, *Langmuir* **1998**, *14*, 5154.
[210] B. J. Liu, T. Torimoto, H. Yoneyama, *J. Photochem. Photobiol. A.* **1998**, *113*, 93.
[211] H. Kisch, P. Lutz, *Photochem. Photobiol. Sci.* **2002**, *1*, 240.
[212] P. Praus, O. Kozak, K. Koci, A. Panacek, R. Dvorsky, *J. Colloid. Interf. Sci.* **2011**, *360*, 574.
[213] Y. S. Chaudhary, T. W. Woolerton, C. S. Allen, J. H. Warner, E. Pierce, S. W. Ragsdale, F. A. Armstrong, *Chem. Commun.* **2012**, *48*, 58.
[214] X. Li, J. T. Chen, H. L. Li, J. T. Li, Y. T. Xu, Y. J. Liu, J. R. Zhou, *J. Nat. Gas Chem.* **2011**, *20*, 413.
[215] X. V. Zhang, S. T. Martin, C. M. Friend, M. A. A. Schoonen, H. D. Holland, *J. Am. Chem. Soc.* **2004**, *126*, 11247.
[216] J.-Y. Liu, B. Garg, Y.-C. Ling, *Green. Chem.* **2011**, *13*, 2029.
[217] T. Arai, S. Tajima, S. Sato, K. Uemura, T. Morikawa, T. Kajino, *Chem. Commun.* **2011**, *47*, 12664.
[218] B. Kumar, J. M. Smieja, C. P. Kubiak, *J. Phys. Chem. C* **2010**, *114*, 14220.
[219] R. Liu, G. B. Yuan, C. L. Joe, T. E. Lightburn, K. L. Tan, D. W. Wang, *Angew. Chem. Int. Ed.* **2012**, *51*, 6709.
[220] R. Liu, C. Stephani, J. J. Han, K. L. Tan, D. W. Wang, *Angew. Chem. Int. Ed.* **2013**, *52*, 4225.
[221] T. Arai, S. Sato, K. Uemura, T. Morikawa, T. Kajino, T. Motohiro, *Chem. Commun.* **2010**, *46*, 6944.
[222] S. Sato, T. Arai, T. Morikawa, K. Uemura, T. M. Suzuki, H. Tanaka, T. Kajino, *J. Am. Chem. Soc.* **2011**, *133*, 15240.
[223] T. Arai, S. Sato, T. Kajino, T. Morikawa, *Energy Environ. Sci.* **2013**, *6*, 1274.
[224] E. E. Barton, D. M. Rampulla, A. B. Bocarsly, *J. Am. Chem. Soc.* **2008**, *130*, 6342.
[225] A. J. Nozik, M. C. Beard, J. M. Luther, M. Law, R. J. Ellingson, J. C. Johnson, *Chem. Rev.* **2010**, *110*, 6873.
[226] D. V. Talapin, J. S. Lee, M. V. Kovalenko, E. V. Shevchenko, *Chem. Rev.* **2010**, *110*, 389.
[227] I. Gur, N. A. Fromer, M. L. Geier, A. P. Alivisatos, *Science* **2005**, *310*, 462.
[228] J. R. Darwent, P. Douglas, A. Harriman, G. Porter, M. C. Richoux, *Coord. Chem. Rev.* **1982**, *44*, 83.
[229] K. Kalyanasundaram, *Coord. Chem. Rev.* **1982**, *46*, 159.
[230] P. V. Kamat, K. Tvrdy, D. R. Baker, J. G. Radich, *Chem. Rev.* **2010**, *110*, 6664.
[231] C. A. Mirkin, R. L. Letsinger, R. C. Mucic, J. J. Storhoff, *Nature* **1996**, *382*, 607.

[232] J. M. Nedeljkovic, M. T. Nenadovic, O. I. Micic, A. J. Nozik, *J. Phys. Chem.* **1986**, *90*, 12.
[233] L. G. Wang, S. J. Pennycook, S. T. Pantelides, *Phys. Rev. Lett.* **2002**, *89*.
[234] L. Cao, S. Sahu, P. Anilkumar, C. E. Bunker, J. A. Xu, K. A. S. Fernando, P. Wang, E. A. Guliants, K. N. Tackett, Y. P. Sun, *J. Am. Chem. Soc.* **2011**, *133*, 4754.
[235] A. Kudo, Y. Miseki, *Chem. Soc. Rev.* **2009**, *38*, 253.
[236] W. Choi, A. Termin, M. R. Hoffmann, *Angew. Chem.* **1994**, *106*, 1148.
[237] S. C. Yan, J. J. Wang, H. L. Gao, N. Y. Wang, H. Yu, Z. S. Li, Y. Zhou, Z. G. Zou, *Adv. Funct. Mater.* **2013**, *23*, 1839.
[238] H. M. Zhu, N. H. Song, W. Rodriguez-Cordoba, T. Q. Lian, *J. Am. Chem. Soc.* **2012**, *134*, 4250.
[239] H. L. Li, Y. G. Lei, Y. Huang, Y. P. Fang, Y. H. Xu, L. Zhu, X. Li, *J. Nat. Gas Chem.* **2011**, *20*, 145.
[240] H. Tong, S. X. Ouyang, Y. P. Bi, N. Umezawa, M. Oshikiri, J. H. Ye, *Adv. Mater.* **2012**, *24*, 229.
[241] X. B. Chen, C. Li, M. Gratzel, R. Kostecki, S. S. Mao, *Chem. Soc. Rev.* **2012**, *41*, 7909.
[242] J. T. Hu, T. W. Odom, C. M. Lieber, *Acc. Chem. Res.* **1999**, *32*, 435.
[243] C. T. Campbell, C. H. F. Peden, *Science* **2005**, *309*, 713.
[244] D. C. Sorescu, W. A. Al-Saidi, K. D. Jordan, *J. Chem. Phys.* **2011**, *135*.
[245] D. C. Sorescu, J. Lee, W. A. Al-Saidi, K. D. Jordan, *J. Chem. Phys.* **2012**, *137*.
[246] a) C. Wang, Z. G. Xie, K. E. deKrafft, W. L. Lin, *J. Am. Chem. Soc.* **2011**, *133*, 13445; b) J. L. Wang, C. Wang, W. B. Lin, *ACS Catal.* **2012**, *2*, 2630.
[247] Y. H. Fu, D. R. Sun, Y. J. Chen, R. K. Huang, Z. X. Ding, X. Z. Fu, Z. H. Li, *Angew. Chem. Int. Ed.* **2012**, *51*, 3364.
[248] D. R. Sun, Y. H. Fu, W. J. Liu, L. Ye, D. K. Wang, L. Yang, X. Z. Fu, Z. H. Li, *Chem. Eur. J.* **2013**, *19*, 14279.
[249] S. C. Yan, Z. Q. Wang, Z. S. Li, Z. G. Zou, *J. Mater. Chem.* **2011**, *21*, 5682.
[250] Y. S. Bae, R. Q. Snurr, *Angew. Chem. Int. Ed.* **2011**, *50*, 11586.
[251] M. Takeuchi, S. Sakai, A. Ebrahimi, M. Matsuoka, M. Anpo, *Top. Catal.* **2009**, *52*, 1651.
[252] L. Q. Ma, C. Abney, W. B. Lin, *Chem. Soc. Rev.* **2009**, *38*, 1248.
[253] A. Phan, C. J. Doonan, F. J. Uribe-Romo, C. B. Knobler, M. O'Keeffe, O. M. Yaghi, *Acc. Chem. Res.* **2010**, *43*, 58.
[254] H. G. Yang, C. H. Sun, S. Z. Qiao, J. Zou, G. Liu, S. C. Smith, H. M. Cheng, G. Q. Lu, *Nature* **2008**, *453*, 638.
[255] G. Liu, J. C. Yu, G. Q. Lu, H. M. Cheng, *Chem. Commun.* **2011**, *47*, 6763.
[256] V. P. Indrakanti, J. D. Kubicki, H. H. Schobert, *Energy Fuel.* **2008**, *22*, 2611.
[257] J. Q. Yu, A. Kudo, *Adv. Funct. Mater.* **2006**, *16*, 2163.
[258] N. Ahmed, Y. Shibata, T. Taniguchi, Y. Izumi, *J. Catal.* **2011**, *279*, 123.
[259] K. Teramura, S. Iguchi, Y. Mizuno, T. Shishido, T. Tanaka, *Angew. Chem. Int. Ed.* **2012**, *51*, 8008.
[260] N. Ahmed, M. Morikawa, Y. Izumi, *Catal. Today.* **2012**, *185*, 263.
[261] X. C. Wang, K. Maeda, A. Thomas, K. Takanabe, G. Xin, J. M. Carlsson, K. Domen, M. Antonietti, *Nat. Mater.* **2009**, *8*, 76.
[262] G. H. Dong, L. Z. Zhang, *J. Mater. Chem.* **2012**, *22*, 1160.
[263] J. Mao, T. Peng, X. Zhang, K. Li, L. Ye, L. Zan, *Catal. Sci. Technol.* **2013**, *3*, 1253.
[264] R. M. Navarro, M. C. Alvarez-Galvan, J. A. V. de la Mano, S. M. Al-Zahrani, J. L. G. Fierro, *Energy Environ. Sci.* **2010**, *3*, 1865.
[265] S. Linic, P. Christopher, D. B. Ingram, *Nat. Mater.* **2011**, *10*, 911.
[266] W. Tu, Y. Zhou, Z. Zou, *Adv. Funct. Mater.* **2013**, *23*, 4996.
[267] K. Sekizawa, K. Maeda, K. Domen, K. Koike, O. Ishitani, *J. Am. Chem. Soc.* **2013**, *135*, 4596.